JOURNAL OF GEOPHYSICAL RESEARCH, VOL. 104, NO. D24, PAGES 31,389–31,409, DECEMBER 27, 1999

A new multiple-band solar radiative parameterization for general circulation models

S. M. Freidenreich and V. Ramaswamy

Geophysical Fluid Dynamics Laboratory, NOAA, Princeton, New Jersey

Abstract. An extensive set of line-by-line plus doubling-adding reference computations for both clear and overcast skies has been utilized to develop, calibrate, and verify the accuracy of a new multiple-band solar parameterization, suitable for use in atmospheric general circulation models. In developing this parameterization the emphasis is placed on reproducing accurately the reference absorbed flux in clear and overcast atmospheres. In addition, a significantly improved representation of the reference stratospheric heating profile, in comparison with that derived from older, broadband solar parameterizations, has been attained primarily because of an improved parameterization of CO_2 heating. The exponential-sum-fit technique is used to develop the parameterization of water vapor transmission in the main absorbing bands. An absorptivity approach is used to represent the heating contributions by CO_2 and O_2, and a spectral averaging of the continuum-like properties is used to represent the O_3 heating. There are a total of two pseudomonochromatic intervals needed to do the radiative transfer problem in the vertically inhomogeneous atmosphere is 72. The delta-Eddington method is used to solve for the reflection and transmission of the homogeneous layers, while the "adding" method is used to combine the layers. The single-scattering properties of the homogeneous layers can account for all types of scattering and absorbing constituents (molecules, drops, ice particles, and aerosols), given their respective single-scattering properties and mass concentrations. With respect to the reference computational results the clear-sky heating rates are generally accurate to within 10%, and the atmospheric absorbed flux is accurate to within 2%. An analysis is made of the factors contributing to the error in the parameterized cloud absorption in the near infrared. Derivation of the representative drop coalbedo for a band using the mean reflection for an infinitely thick cloud (thick-averaging technique) generally results in a better agreement with the reference cloud absorbed flux than that derived using the mean drop coalbedo (thin-averaging technique), except for high, optically thin water clouds. Further, partitioning the $2500 < \nu < 8200$ cm^{-1} spectral region into several more bands than two (the minimum required) results in an improved representation of the cloud absorbed flux, with a modest increase in the shortwave radiation computational time. The cloud absorbed flux is accurate to within 10%, and the cloudy layer heating rates are accurate to within 15%, for water clouds, while larger errors can occur for ice clouds. The atmospheric absorbed, downward surface, and upward top-of-the-atmosphere fluxes are generally accurate to within 10%.

1. Introduction

For clear atmospheres the requirement for efficient and accurate solar radiative parameterizations in general circulation models (GCMs) is met by the use of broadband formulations of gaseous absorption [*Lacis and Hansen*, 1974; *Sasamori*, 1972; *Ramaswamy and Freidenreich*, 1992, hereinafter RF92]. For overcast atmospheres, where drops and gas (mainly water vapor) are both present, the formulation of an accurate solar parameterization, using the broadband concept, is much more difficult. This is especially the case when only one near-infrared interval is utilized. The spectral absorption strengths of both constituents vary substantially, particularly in the near-infrared, and especially for water vapor. Although drop absorption can be well represented in terms of broadband-specified quantities, for example, reflection and transmission (RF92), the presence of water vapor introduces spectral dependences that cannot be easily accounted for in a general sense using the broadband concept. As discussed by RF92, water vapor influences the solar flux absorbed by a cloud in two principal ways: (1) the spectrally dependent attenuation of the solar beam above the topmost cloud layer affects the spectral flux available to be absorbed by the cloud, especially by low clouds; and (2) the spectrally dependent absorption by vapor inside a cloud enhances the overall cloud absorptivity. Thus the accuracy in parameterizing the total amount of solar flux that a cloudy atmosphere will absorb is affected by the manner in which the simultaneous spectral variations in drop and vapor absorption strengths are taken into account. A typical broadband approach seeks to maximize the spectral width in order to achieve computational efficiency.

Several attempts have been made to parameterize drop plus water vapor absorption using the broadband concept, accounting in some way or the other for the effect of the simultaneous spectral variation of both entities. RF92, to parameterize drop

Paper number 1999JD900456.

absorption, determine the reflection and transmission properties of a drop-only atmosphere in specific bands using the delta-Eddington (DE) [*Joseph et al*., 1976] method and then spectrally averaged them to obtain the representative values for the water vapor absorbing region of the spectrum. A modified form of the Lacis-Hansen [*Lacis and Hansen*, 1974] formulation (RF92) is used to parameterize water vapor transmission. To account for the spectrally dependent attenuation of the solar beam by water vapor above a cloud, a computational scheme is used to alter systematically the drop-only broadband values of reflection and transmission. Absorption of solar radiation inside the cloud is handled by assuming that the total broadband transmission is the product of those due to drops and those due to vapor.

Briegleb [1992] (hereinafter BR92) developed a simple formulation for treating drop plus vapor absorption. Utilizing *Slingo*'s [1989] four-band drop specifications and a slightly altered form of the Lacis-Hansen vapor parameterization, each absorption coefficient due to vapor is assigned to one of the drop spectral bands. Although this is still a broadband formulation, there is some accounting of the simultaneous spectral variations in the absorption strength due to drops and vapor. In another procedure, *Li et al*. [1997] modified the solar spectral weights of *Slingo*'s [1989] 24-band drop formulation to account for the spectrally dependent gaseous absorption above low clouds. Then the spectrally averaged drop reflection and transmission could be used, with an appropriate broadband vapor parameterization, to estimate the solar absorption, similar to RF92.

Using line-by-line (hereinafter LBL) results, the error in cloud-absorbed flux that results from the prescription by RF92 was investigated for a variety of overcast sky situations. That procedure works quite well in correcting the overestimate in the low cloud solar absorption resulting from the application of the broadband drop reflection and transmission values. However, as the number of contiguous cloudy layers increases (geometrical thickness increases), the underestimate in cloud absorption becomes more pronounced. This is due to the manner of the broadband treatment of the enhanced absorption by vapor inside the cloud. Overall, errors in the cloud-absorbed flux of up to 40 W m^{-2} can occur for an atmosphere containing a single cloud. Even larger errors were seen to occur when consideration was given to an atmosphere containing multiple cloudy layers that are noncontiguous. Thus some uncertainty remains in employing this procedure in a general way.

In spite of its simplicity the BR92 formulation is also found to work quite well in reproducing the reference cloud solar absorption for a variety of overcast sky conditions. However, similar to the difficulties encountered in RF92, it can also produce large errors for an atmosphere containing a geometrically thick cloud or multiple clouds. This will be highlighted later. The *Li et al*. [1997] prescription is likewise useful for computing the absorption in a single-layer cloud; however, uncertainties remain with regard to its applicability to atmospheres containing multiple cloud layers.

It is clear from the weaknesses of the general broadband framework that a more detailed partitioning of the solar spectrum is needed to reduce large errors in the parameterized solar absorption that can arise in specific overcast sky cases. Thus, in order to improve upon the results of the earlier, simpler formulations a multiple-band approach is adopted and discussed in this study. This procedure allows for a more explicit consideration of the simultaneous spectral variation in the absorption strength of drops and water vapor and its effect on the parameterized cloud absorption in the near-infrared. Also, the multiple-band technique allows for a better and a more transparent representation of the simultaneous spectral variation of O_3 absorption, absorption and scattering by cloud drops, absorption and scattering by aerosols, and molecular scattering in the visible and ultraviolet regions.

In section 2 we discuss the sources of data used to develop the reference results. In section 3 we discuss the reference results for the individual gases. In section 4 we present the methodology used to parameterize the solar absorption and scattering by the gases and other constituents. In section 5, we discuss the factors dictating the partitioning of the solar spectrum into bands. Also, a detailed investigation is made of the sensitivity of the parameterized cloud absorption to various factors in different regions of the near-infrared spectrum. In section 6 we discuss the parameters involved in the new formulation. In sections 7 and 8 we discuss the errors that arise because of the new multiple-band parameterization for clear-sky and overcast atmospheres, respectively. In section 9 we highlight the important conclusions resulting from this study.

2. Computational Model

The radiative transfer model used for the "benchmark" computations has a high vertical resolution, dividing the atmosphere into 122 layers and spanning the pressure levels from 10^{-3} to 1013.25 mbar, as described by *Schwarzkopf and Fels* [1991]. In this study we consider the effects of gaseous absorption by water vapor, CO_2, O_2, and O_3 and scattering and absorption by air molecules, water drops, and ice particles. The spectral region considered is $0 < \nu < 57{,}600$ cm^{-1}. The LBL method [see *Ramaswamy and Freidenreich*, 1991] is used to determine the reference solar absorption for the portion of the solar spectrum where line parameter data are available, namely, $0 < \nu < 22{,}700$ cm^{-1} and $44{,}100 < \nu < 57{,}600$ cm^{-1}, while a 1 cm^{-1} spectral resolution is used otherwise. Line parameter data are taken from the Air Force Geophysics Laboratory [*Rothman et al*., 1992] compilation for the $0 < \nu < 22{,}700$ cm^{-1} region, corresponding to the spectral limits of water vapor absorption bands, while a more recent compilation (L. S. Rothman, personal communication, 1997) is used for the $44{,}100 < \nu < 57{,}600$ cm^{-1} region (the Schumann-Runge O_2 band). For O_3 absorption the continuum values of the O_3 cross section are taken from *World Meteorological Organization* (*WMO*) [1986], with updated values in part of the ultraviolet [*Jet Propulsion Laboratory* (*JPL*), 1992]. *Labs and Neckel* [1970] solar fluxes are used for $0 < \nu < 50{,}000$ cm^{-1}; however, for larger wavenumbers their specifications are poorer. The *WMO* [1986] values are used for $50{,}000 < \nu < 57{,}000$ cm^{-1}, the upper limit where it is defined, and the *Nicolet* [1989] values are used for $57{,}000 < \nu < 57{,}600$ cm^{-1}. The total incident solar flux is 1358 W m^{-2}. The reference calculations that are used to develop, calibrate, and verify the accuracy of the new multiple-band parameterization assume a midlatitude summer (MLS) [*McClatchey*, 1972] atmospheric profile and a CO_2 amount of 346 ppmv. Computations are also made for other atmospheric profiles and higher CO_2 amounts to verify further the accuracy of the parameterization for clear atmospheres. Most of the reference calculations assume a nonreflecting surface. Results are also considered for various solar zenith angles.

To perform multiple scattering accurately, the doubling-adding (DA) method [*Hunt and Grant*, 1969] is employed for

the reference (LBL + DA) calculations. Details with regards to implementation of the DA technique are described by *Ramaswamy and Freidenreich* [1991] for the case of drops. With the incorporation of Rayleigh scattering in the present study, two additional details are noted. First, the Rayleigh phase function is expanded into a three-term Legendre polynomial set to represent the scattering; it contains a slight correction for molecular anisotropy, with the depolarization factor set to 0.0139 [*McCartney*, 1976]. Second, the resultant phase function for drops plus Rayleigh scattering is a sum of that for each constituent, weighted by the ratio of the scattering optical depth for that constituent to the total. This resultant phase function is used to define the initial reflection and transmission matrices required by the doubling algorithm.

For overcast sky cases the spectral dependence of the drop single-scattering properties is derived using either *Slingo*'s [1989] 24-band parameterization or the containing small (CS) and containing large (CL) specifications from the Intercomparison of Radiation Codes in Climate Models (ICRCCM) project [*Fouquart et al*., 1991]. For ice crystals a formulation developed by *Fu* [1996] is used. In this paper we focus on water clouds in the development of the new parameterization, but the results as applied to ice clouds are also analyzed. The drop optical depth is specified at a reference wavelength ($\lambda = 0.55$ μm). The DE algorithm is used to treat the multiple-scattering problem in the parameterization.

3. Reference Results for Gaseous Absorption

Before discussing the development of the formulations for representing the solar absorption by the individual gases it is useful to compare where, and to what magnitude, each of them contribute to the atmospheric heating. Figure 1 displays the vertical profiles of heating rate in a MLS atmosphere for overhead sun conditions (0°). Also shown is the corresponding total clear-sky heating rate profile accounting for all gases and including Rayleigh scattering. Mostly because of overlapping of absorption among the various gases, the total clear-sky heating rate differs somewhat (~15% or less) from the corresponding result derived by summing the individual heating rate contributions. Thus, although an exact quantitative assessment of the relative contribution by each gas is not possible, a qualitative one can be made.

Water vapor is the primary contributor to tropospheric heating for $P > 200$ mbar, with the other gases contributing considerably less. For $100 < P < 200$ mbar, water vapor, CO_2, and O_3 make the most significant contributions to the total heating. O_3 becomes the dominant contributor to the heating in the lower stratosphere, while the contribution by water vapor becomes less important with height. O_3 is the dominant contributor to heating throughout the stratosphere, up to ~0.02 mbar. For $P < 0.02$ mbar, first CO_2 and then, with increasing altitude, O_2 dominates the solar heating, the latter arising principally because of the Schumann-Runge absorption band in the ultraviolet.

The relative contribution to the total atmospheric heating by each gas individually affects the degree of accuracy needed to parameterize it. Water vapor requires an accurate representation of its heating rate dependence with height in order to account properly for tropospheric absorption. The significantly smaller contributions by the other gases there imply that a lesser degree of accuracy is affordable in parameterizing their effects. For the upper troposphere and lower stratosphere it is important to represent accurately the total heating rate profile in order to simulate properly the temperatures there. This is due to a large radiative time constant at these altitudes and hence a greater sensitivity to small heating rate biases. An accurate representation of the O_3 heating is easy to achieve because of its continuum nature, but it is more difficult to parameterize accurately the lower stratospheric heating effects because of the other gases, as described below. Further, the large increase in heating due to CO_2 and O_2 in the remainder of the stratosphere must also be represented accurately.

Freidenreich and Ramaswamy [1993] (hereinafter FR93) show that use of the Lacis-Hansen and Sasamori formulations

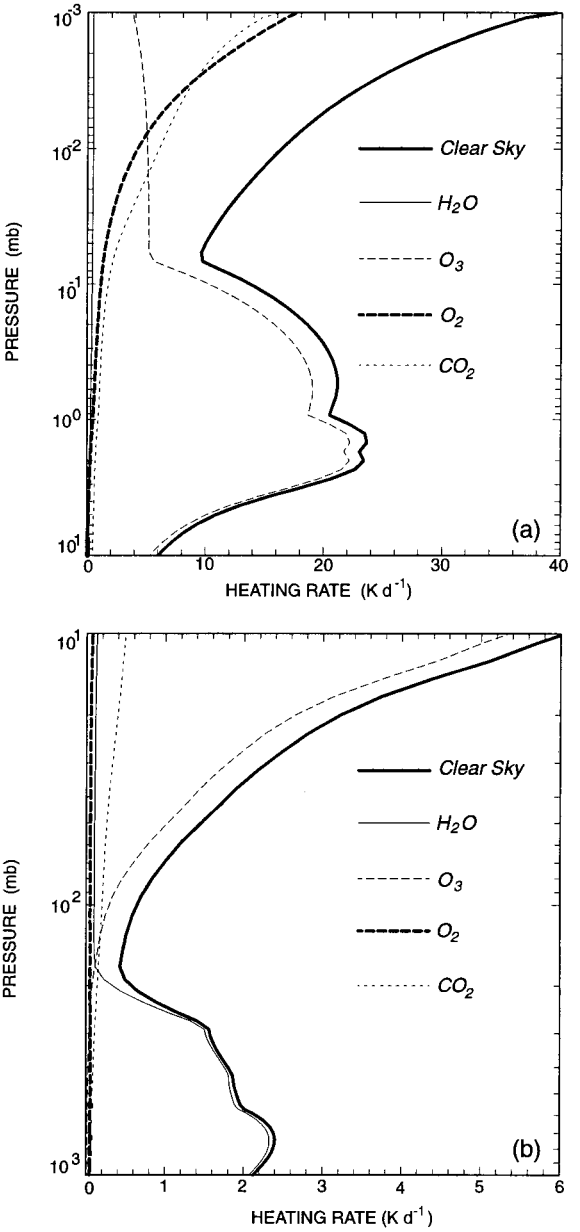

Figure 1. The reference solar heating rate profiles for (a) $P < 10$ mbar and (b) $P > 10$ mbar for water vapor, CO_2, O_2, and O_3. Also shown is the clear-sky result for all gases with Rayleigh scattering. A midlatitude summer (MLS) atmosphere and an overhead sun are considered, and the CO_2 amount is 346 ppmv.

for water vapor and CO_2, respectively, leads to an increasing underestimate of the reference heating with height in the stratosphere. Since the FR93 study the CO_2 stratospheric heating rate has been found to be considerably larger, with the departure from the earlier computation increasing with height. Upon further investigation (J. Eluszkiewicz, personal communication, 1995), in the previous LBL computations, erroneous values (mostly zero) of the gas optical depth were assigned to frequencies within 0.1 cm^{-1} of an absorption line. The same inaccuracy is noted for the stratospheric heating due to water vapor, but the increased heating that results in that case is relatively quite small. Thus the underestimate in the reference stratospheric heating due to the Lacis-Hansen and Sasamori formulations is greater than that determined previously. Further, *Freidenreich and Ramaswamy* [1995], using a fixed dynamical heating model, show that an increase in the lower stratospheric temperatures occurs because of an improved accounting of the heating effects of CO_2 and water vapor. These results were based on formulations utilizing the older reference calculations. Notably greater temperature increases would be expected to occur when the increased heating presented in Figure 1 is taken into account. This further emphasizes the need to develop formulations that properly represent gaseous absorption in the stratosphere.

The failure of some formulations to simulate adequately the stratospheric heating may be due in part to inaccuracies in the computation of absorption associated with small absorber amounts upon which the formulations are derived. Another factor that is discussed in the next section is how the absorber amounts are scaled with height. This scaling is used to simulate the pressure dependence of the LBL-derived absorption coefficient.

4. Methods to Parameterize Absorption and Scattering

4.1. Water Vapor

To parameterize the absorption due to water vapor, we use the exponential sum fit (ESF) technique [*Wiscombe and Evans*, 1977]. In this study the averaged transmission in a band, defined between ν_1 and ν_2 cm^{-1}, is determined as a function of the vapor amount, using the LBL-derived transmission at each monochromatic frequency point:

$$T^{\mathrm{LBL}}_{\mathrm{H_2O}}(P_0, w) = \frac{\sum_{\nu=\nu_1}^{\nu_2} S_\nu \exp\left[-k'_\nu(P_0, T_0)w\right]}{\sum_{\nu=\nu_1}^{\nu_2} S_\nu}, \qquad (1)$$

where $T^{\mathrm{LBL}}_{\mathrm{H_2O}}$ is the band-averaged transmission, w is an arbitrary vapor amount, k'_ν is the monochromatic absorption coefficient, S_ν is the monochromatic spectral solar irradiance at the top of the atmosphere (hereinafter TOA), P_0 is a reference pressure, and T_0 is a reference temperature. We consider the reference pressure P_0 to be anywhere from 1 to 1013 mbar, depending on the band, as explained below. For instance, a stratospheric pressure value of P_0 is found to be necessary for an accurate representation of upper tropospheric heating in the strongest absorbing bands. T_0 is fixed at 273 K. $T^{\mathrm{LBL}}_{\mathrm{H_2O}}$ is fitted by a sum of exponentials using a nonlinear least squares routine:

$$T^{\mathrm{LBL}}_{\mathrm{H_2O}} \cong \sum_{i=1}^{n} a_i \exp\left(-k_i w\right), \qquad (2)$$

where a_i, k_i are a set of weights and pseudomonochromatic absorption coefficients, respectively, and n is the number of terms used to fit the transmission. The term "pseudo" is used because the derived coefficients do not depict the actual spectral distribution of absorption strengths in the band interval but are treated as fictitious spectral absorption coefficients for the purpose of the radiative transfer calculations in that band. Henceforth, we use the designation (a, k) to refer to such a derived set. Several sets of (a, k), which result in a large catalog of potential ESFs, are derived for each n and P_0.

For the inhomogeneous atmosphere, and when applied to a particular model layer l, the parameterized band transmission $T_{\mathrm{H_2O},l}$ can be written as

$$T_{\mathrm{H_2O},l} = \sum_{i=1}^{n} a_i \exp\left[-k_i \frac{W'_{\mathrm{H_2O},l}}{\mu_0}\right] = \sum_{i=1}^{n} a_i \exp\left[-\frac{\tau_{\mathrm{H_2O},i,l}}{\mu_0}\right], \qquad (3)$$

where μ_0 is the cosine of the solar zenith angle and $\tau_{\mathrm{H_2O},i,l}$ are the pseudomonochromatic water vapor optical depths. $W'_{\mathrm{H_2O},l}$ is the scaled water vapor amount defined as

$$W'_{\mathrm{H_2O},l} = 10 R_{\mathrm{H_2O},l}\left(\frac{P_l}{P_0}\right)^m \left(\frac{P_{L+1} - P_L}{g_0}\right) \qquad (4)$$

$R_{\mathrm{H_2O},l}$ is the vapor mass mixing ratio (g/g); P_l denotes the mean layer pressure (mbar); $(P_l/P_0)^m$ is the pressure scaling, with m being the scaling exponent $(0 < m < 1)$; g_0 is the acceleration due to gravity (m s^{-2}); and L and $(L + 1)$ refer to the pressure level values that define layer l, with level L above level $(L + 1)$. The absorber amount resulting from (4) is in g cm^{-2}. A pressure scaling is needed to account for the dependence of k'_ν on pressure in the inhomogeneous atmosphere. Note that in this study, no scaling is done to account for the temperature dependence of k'_ν. It is found that the atmospheric absorption in an inhomogeneous atmosphere can be adequately parameterized by considering the pressure dependence only. The μ_0 is set to 0.6 for the purposes of comparing it with the reference result and for choosing the optimal (a, k) for the parameterization.

In practice, it is not difficult to find a set (a, k) that accurately fits the transmission at a pressure P_0. In this study, however, we judge the adequacy of using a derived set by how well its use contributes, together with the choices of P_0 and m, toward an accurate fit of the LBL-determined tropospheric heating rate profile in the band for the MLS atmosphere. Thus we examine the accuracy of the derivative of transmission (i.e., flux convergence), rather than transmission itself, in assessing the worthiness of a given ESF. This sets up a more stringent condition for testing the accuracy of the parameterized heating rates.

In selecting a specific (a, k) from the catalog for each band we determine for each n the (a, k) and m and P_0 that produce a tropospheric heating rate profile that best fits the reference one. A best fit is defined as the minimum value of the error in the sum of the squares. We seek to restrict the size of n in any particular band by considering a large number of ESFs along with variations in P_0 and m. In general, the number of terms needed to represent adequately the heating in any particular

band increases as the strength of the absorption increases. In deciding upon the final ESF in each band where the technique is used the error in the tropospheric heating rate as a function of n is examined. Also, the total number of pseudomonochromatic intervals for all such bands and the resultant error in the corresponding total heating rate profile are examined. After all of the above scrutiny the optimal (a, k), m, and P_0 for each of these bands are selected.

There are two instances where the ESF technique is not used. First, for any band where water vapor is weakly absorbing, only one pseudomonochromatic absorption coefficient is needed. In this instance the coefficient is derived by determining the value that results in a best fit to the reference tropospheric heating profile. In these bands the pressure scaling is ignored ($m = 0$) in determining the column water vapor amounts since the transmission is virtually independent of the P_0 chosen. Second, the technique does not produce satisfactory fits to the reference heating profile in the lower stratosphere for the bands located in the strongest absorbing regions. The selection of appropriate P_0 and m for proper representation of the tropospheric heating causes the scaled water vapor amounts to decrease rapidly with height in the stratosphere; this results in the stratospheric heating being increasingly underestimated with height. This is another factor that can explain the underestimate in stratospheric heating produced by some commonly used broadband formulations. Because of the importance of accurately simulating the lower stratospheric heating, we seek to improve upon the heating rates determined for $10 < P < 100$ mbar in these strongly absorbing bands as follows. An additional pseudomonochromatic absorption coefficient and weight (stipulated to be small in magnitude) are incorporated in the ESF already chosen for each of these bands. The values selected are those that produce a best fit to the reference heating rate for $10 < P < 100$ mbar. Since this additional term is a correction factor for the derived ESF, there is no dependence of its transmission contribution on the P_0 selected. Thus the pressure scaling is again ignored in determining the transmission contribution by this additional term. To compensate for this additional weight, an adjustment is made in the weight of one of the other terms in the ESF. This adjustment involves only a small change in the magnitude of the weights concerned.

4.2. CO_2 and O_2

The ESF method could also be used to find an expression that represents well the tropospheric absorption by CO_2 and O_2, but their minor contributions to the overall tropospheric heating (Figure 1) do not justify the computational cost involved. A simple formulation for both gases is found that adequately represents both the absorbed solar flux in the troposphere and the increase of solar heating with height in the upper stratosphere. In the following discussion, x refers to either CO_2 or O_2. The transmission due to gas x in a band between the TOA and a particular model layer l is represented by

$$T_{x,l} = (1 - \alpha_{x,l}) = (1 - \alpha_{1,x,l})(1 - \alpha_{2,x,l}), \tag{5}$$

where $T_{x,l}$ is the column transmission and $\alpha_{x,l}$ is the column absorption, which depends on $\alpha_{1,x,l}$ and $\alpha_{2,x,l}$, as defined below. For a well-mixed gas the scaled column path length (in cm-atm) from the TOA to a layer l, given a value of the scaling factor m and accounting for the slant absorption path, is given by

$$W'_{x,l} = 10^4 \frac{R_x}{g_0 \rho_0 \mu_0} \int_0^{P_l} \left(\frac{P}{P_0}\right)^m dP = 10^4 \frac{R_x}{g_0 \rho_0 \mu_0 P_0^m} \left(\frac{P_l^{m+1}}{m+1}\right), \tag{6}$$

where R_x is the volume mixing ratio, ρ_0 is the surface level air density (kg m^{-3}), P_0 is set to 1013 mbar, $\alpha_{1,x,l}$ and $\alpha_{2,x,l}$ use the unscaled ($m = 0$) and scaled (with m set to 1) column path lengths, $W_{x,l}$ and $W'_{x,l}$, respectively, and are defined as

$$\alpha_{1,x,l} = a_x[(1 + b_x W_{x,l})^{c_x} - 1] \tag{7}$$

$$\alpha_{2,x,l} = d_x[(1 + e_x W'_{x,l})^{f_x} - 1], \tag{8}$$

and a_x, b_x, c_x, d_x, e_x, and f_x are constants. First, the coefficients a_x, b_x, and c_x for $\alpha_{1,x,l}$ are chosen to define a best fit to the reference heating profiles from the TOA to a pressure value in the stratosphere when $\alpha_{2,x,l} = 0$. Three solar zenith angles, 0°, 53°, and 75°, are considered, and the best fit is defined as that which yields the smallest maximum relative error among all three cases. Then the coefficients d_x, e_x, and f_x for $\alpha_{2,x,l}$ are chosen to define a best fit to the reference heating profiles for the entire atmosphere when the fit for $\alpha_{1,x,l}$ is applied. Thus the formulation for $\alpha_{2,x,l}$ is designed to reduce the residual error in the heating rate that results in both the lower stratosphere and the troposphere from the application of the formulation for $\alpha_{1,x,l}$. To incorporate absorption in a scattering atmosphere, an "effective" gas optical depth is defined in a particular model layer l as

$$\tau_{x,l} = -\mu_0 \ln\left[\frac{T_{x,(L+1)}}{T_{x,L}}\right] \tag{9}$$

4.3. O_3

Because of the continuum nature of O_3 absorption, only a single exponential term (or equivalently one pseudomonochromatic interval) is required to represent the heating rate profile in the band. A value of the absorption coefficient is chosen that minimizes the maximum relative error in the heating rate, compared to the reference calculation, for a zenith angle of 53°. The accuracy of its parameterization is dictated by the spectral band width chosen. The resulting gas optical depth in a particular model layer l is determined by multiplying this value by the O_3 amount in the layer:

$$\tau_{O_3,l} = k_{O_3} W_{O_3,l} \tag{10}$$

$$W_{O_3,l} = 10 R_{O_3,l}\left(\frac{P_{L+1} - P_L}{g_0}\right) \tag{11}$$

where k_{O_3} is the absorption coefficient (cm^2 g^{-1}) defined at STP, W_{O_3} is the amount in g cm^{-2}, and R_{O_3} is the O_3 mass mixing ratio.

The total gas optical depth in a particular model layer l at each pseudomonochromatic frequency is given as the sum of the optical depths for the individual constituents. The resulting transmission in any band where two or more gases are simultaneously absorbing is thus given by the product of the transmission due to each gas.

4.4. Rayleigh Scattering

Rayleigh scattering [*McCartney*, 1976] is incorporated by determining the optical depth at a reference wavenumber within the band spectral interval. To determine the reference wavenumber, the solar weighted mean transmissivity at the

surface and reflectivity at the TOA are determined for each band spectral interval using a 1 cm^{-1} resolution version of the LBL model and assuming an atmosphere containing only Rayleigh scattering. A solar zenith angle of 53° is also assumed. The reference wavenumber selected is that which results in a transmissivity and reflectivity that best agrees with the band-averaged values. Thus, like O_3, the band spectral width chosen determines the accuracy of its representation when compared to the reference calculation. Given the value of the scattering coefficient at the reference wavenumber, computed for the surface pressure (P_{sfc}) and temperature (T_{sfc}) of the MLS profile (1013.25 mbar and 293.78 K, respectively), the value of the Rayleigh optical depth for a model layer l is then

$$\tau_{\text{Rayleigh},l} = k_{\text{Rayleigh}}\left(\frac{P_{L+1} - P_L}{\rho_l g_0}\right)\left(\frac{P_l}{P_{\text{sfc}}}\right)\left(\frac{T_{\text{sfc}}}{T_l}\right), \qquad (12)$$

where k_{Rayleigh} is the scattering coefficient in m^{-1}.

4.5. Cloud Properties

The drop extinction (scattering plus absorption) coefficient and asymmetry factor are defined as the solar weighted mean value over the band spectral interval:

$$\overline{k_{\text{drop}}} = \frac{\sum_{\nu=\nu_1}^{\nu_2} k_{\text{drop},\nu} S_\nu}{\sum_{\nu=\nu_1}^{\nu_2} S_\nu} \qquad (13)$$

$$\overline{g_{\text{drop}}} = \frac{\sum_{\nu=\nu_1}^{\nu_2} g_{\text{drop},\nu}\omega_{\text{drop},\nu}k_{\text{drop},\nu} S_\nu}{\sum_{\nu=\nu_1}^{\nu_2} \omega_{\text{drop},\nu}k_{\text{drop},\nu} S_\nu} \qquad (14)$$

Given a specified value of the drop optical depth (τ_{drop}) at the reference wavenumber ν_0 (18,182 cm^{-1}, equivalent to 0.55 μm wavelength), the corresponding value in any band is related as

$$\overline{\tau_{\text{drop}}} = \frac{\overline{k_{\text{drop}}}}{k_{\text{drop},\nu_0}} \times \tau_{\text{drop}} \qquad (15)$$

For the drop single-scattering albedo, or coalbedo, two methods highlighted by *Edwards and Slingo* [1996, hereinafter ES96] are investigated here, referred to as the thin-averaging and thick-averaging techniques. In the thin-averaging technique the representative drop coalbedo is defined as the solar weighted mean value over the band spectral interval:

$$\overline{\omega_{\text{drop}}} = \frac{\sum_{\nu=\nu_1}^{\nu_2} \omega_{\text{drop},\nu}k_{\text{drop},\nu} S_\nu}{\sum_{\nu=\nu_1}^{\nu_2} k_{\text{drop},\nu} S_\nu} \qquad (16)$$

In the thick-averaging technique the representative drop coalbedo is derived from the solar weighted mean reflectivity, assuming an infinitely thick cloud:

$$\overline{\omega_{\text{drop}}} = \frac{4\overline{R^\infty_{\text{drop}}}}{(1 + \overline{R^\infty_{\text{drop}}})^2 - \overline{g_{\text{drop}}}(1 - \overline{R^\infty_{\text{drop}}})^2}, \qquad (17)$$

where

$$\overline{R^\infty_{\text{drop}}} = \frac{\sum_{\nu=\nu_1}^{\nu_2} R^\infty_{\text{drop}} S_\nu}{\sum_{\nu=\nu_1}^{\nu_2} S_\nu}, \qquad (18)$$

and the reflectivity for an infinitely thick cloud R^∞_{drop} is derived using the similarity parameter as outlined by ES96.

4.6. Multiple Scattering Methodology

To derive the fluxes and heating rates in a scattering atmosphere, combination formulas are first used to define the bulk layer properties (τ_l, ω_l, and g_l) considering all absorbing and scattering constituents (e.g., BR92). Note that water vapor in cloud is assumed to be at saturation values. This is done in each pseudomonochromatic interval. Then the layer reflection and transmission values are determined using the DE method. With this multiple-scattering approximation an appropriate adding method [e.g., *Ramaswamy and Bowen*, 1994] is used to obtain the vertical dependence of reflection and transmission in an inhomogeneous atmosphere. The adding method accounts for both the solar direct and diffuse beam interactions with the various constituents in each layer. For bands in which the ESF technique is used these quantities are summed with the appropriate weights applied in order to obtain the representative band values; otherwise, the pseudomonochromatic interval value is equivalent to its band value. The appropriate TOA solar flux is then applied to determine the vertical profile of the downward and upward solar fluxes and the heating rates. These fluxes and heating rates are summed over all bands to obtain the total spectrum values.

5. Partitioning the Solar Spectrum

An important consideration in developing a multiple-band parameterization is the choice of the spectral delimiters defining specific band regions. Figure 2 illustrates the spectral variation of the relevant quantities that needs to be considered in partitioning the spectrum. Figures 2a and 2b illustrate the spectral variation of the gas optical depth and the drop coalbedo for $0 < \nu < 14{,}600$ cm^{-1}, respectively. Figures 2c and 2d display the gas optical depth and the clear-sky reflectivity at the TOA, respectively, for the remainder of the spectral region defined in this study, $14{,}600 < \nu < 57{,}600$ cm^{-1}. The spectral gas optical depth is proportional to the combined absorption strength of the gaseous constituents. The quantity depicted is the vertically integrated value for the atmospheric column, accounting for water vapor, CO_2, O_2, and O_3. However, since water vapor is by far the dominant absorber for $0 < \nu < 14{,}600$ cm^{-1}, the variations presented are virtually those due to vapor alone [see *Ramaswamy and Freidenreich*, 1998; RF92]. For $14{,}600 < \nu < 57{,}600$ cm^{-1}, O_3 becomes the primary absorber, except for $\nu > 47{,}000$ cm^{-1}, where O_2 is the dominant contributor. The drop coalbedo (i.e., 1 minus the single-scattering albedo) is proportional to the drop absorption strength, facilitating comparisons with the simultaneous spectral variation in the gas absorption strength. Although the extinction coefficient and the asymmetry factor also vary spectrally, they are less important contributors to spectral variations in solar absorption across the spectrum [*Ramaswamy and Freidenreich*, 1998]. Two drop size distributions are shown corresponding to the CS

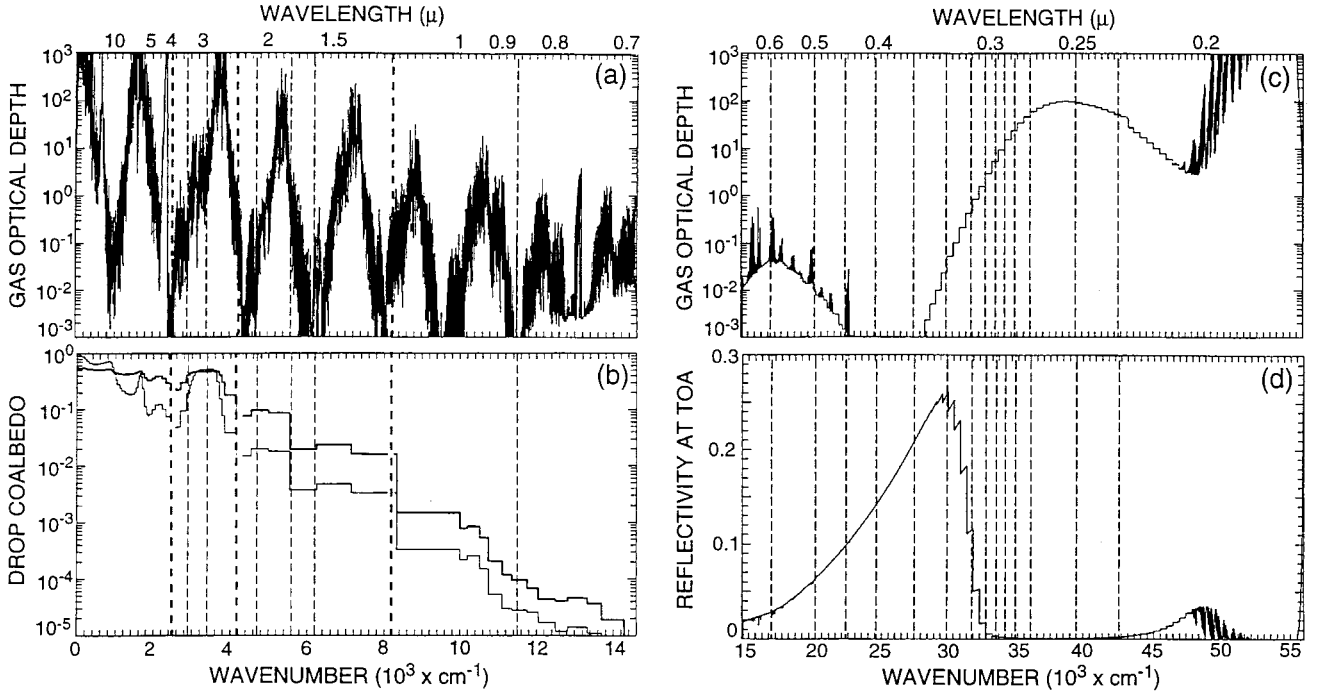

Figure 2. The spectral variation of relevant quantities that are involved in determining how the solar spectrum is partitioned into bands: (a) variation of the total column gas optical depth and (b) drop coalbedo for $0 < \nu < 14{,}600$ cm^{-1} and (c) variation of the total column gas optical depth and (d) clear-sky top-of-the atmosphere (TOA) reflectivity for $14{,}600 < \nu < 57{,}600$ cm^{-1}. Two distributions of drop coalbedo are shown in Figure 2b corresponding to the containing small (CS) (thin-solid line) and containing large (CL) (thick-solid line) drop size distributions [*Fouquart et al.*, 1991]. The spectral band delimiters involved in the new parameterization (thin-dashed line) are superimposed in Figures 2a–2d. The spectral band delimiters chosen for analysis of the error in the cloud absorbed flux (thick-dashed line) are also superimposed in Figures 2a and 2b.

and CL cloud. These drop models illustrate the differing magnitudes of their respective spectral variation in coalbedo. The clear-sky reflectivity at the TOA for the MLS atmosphere is derived assuming an overhead Sun and nonreflecting surface and using the LBL + DA method. This quantity is proportional to the Rayleigh optical depth, but it also accounts for the effect of gaseous absorption. The variations of the quantities presented in Figure 2 guide us in choosing the delimiters for the new multiple-band parameterization in each of the major spectral regions: namely, near-infrared, visible, and ultraviolet.

5.1. Near-Infrared Spectrum

In the near-infrared, Figures 2a and 2b illustrate the variation in magnitude of the vapor and drop absorption strengths. There is a rapid variation in the vapor absorption strength, while that due to drop absorption is more gradual. The spectral variation in cloud absorption is dictated by the much finer variation in the water vapor optical depth, and the degree of accuracy that can be achieved in parameterizing it depends on the choice of the spectral band delimiters.

A series of experiments is conducted in which the cloud-absorbed solar flux from parameterized calculations are compared with a corresponding reference result for specific spectral regions. The error in the parameterized cloud absorption is analyzed, depending on the spectral band delimiters considered in these regions. The results of this analysis are used as a guide in determining the partitioning of the spectrum in the near-infrared. For the parameterization the drop single-scattering properties defined for each band are applied in conjunction with an accurate ESF for the vapor transmission, and the DE and adding methods are used to obtain the cloud absorbed flux, in the manner described in section 4. For the reference result the LBL + DE (rather than the LBL + DA) method is used to obtain the cloud absorbed flux in this section in order to avoid errors in the parameterization arising solely because of differences in the scattering technique. For simplicity, water vapor is the only gas considered to be present along with the cloud drops. Also, the solar zenith angle is fixed at 53°.

To partition systematically the near-infrared spectrum, we start with spectral delimiters that define the principal water vapor absorption bands. Guided by *Ramaswamy and Freidenreich* [1991, Table 2], the delimiters defining the vapor bands are as follows: $0 < \nu < 2500$ cm^{-1}, $2500 < \nu < 4200$ cm^{-1}, $4200 < \nu < 6200$ cm^{-1}, $6200 < \nu < 8200$ cm^{-1}, $8200 < \nu < 9700$ cm^{-1}, $9700 < \nu < 11{,}500$ cm^{-1}, $11{,}500 < \nu < 12{,}900$ cm^{-1}, and $12{,}900 < \nu < 14{,}600$ cm^{-1}. We stipulate that any band(s) chosen for this analysis meet one of the following criteria: (1) it corresponds to these spectral limits, (2) it corresponds to spectral limits resulting from combining two or more consecutive vapor bands, or (3) it corresponds to spectral limits resulting from partitioning a vapor band into smaller subbands. Utilizing these spectral delimiters, four regions are chosen to investigate in detail the error in the parameterized cloud absorbed flux: $0 < \nu < 2500$ cm^{-1}, $2500 < \nu < 4200$ cm^{-1}, $4200 < \nu < 8200$ cm^{-1}, and $8200 < \nu < 14{,}600$ cm^{-1}. The error in the parameterized cloud absorbed flux in these regions is first determined when the spectral band delimiters

Table 1a. The Line-by-Line Plus Delta-Eddington (LBL + DE) Determined Absorbed Solar Flux in the Cloud for $0 < \nu < 2500$ cm^{-1} for an Overcast Atmosphere Containing Only Water Vapor for Drop Optical Depths of 10 and 1

Location, mbar	Type	LBL + DE, W m^{-2}	Relative Error, %: Thin One-Band Case	Relative Error, %: Thick One-Band Case
		$\tau_{drop} = 10$		
800–900	CS	3.1	10	6
	CL	3.8	3	2
180–200	CS	5.6	5	2
	CL	6.7	1	<1
300–800	CS	5.0	4	1
	CL	6.0	<1	<1
		$\tau_{drop} = 1$		
800–900	CS	1.3	12	6
	CL	2.2	5	2
180–200	CS	2.2	9	3
	CL	3.7	2	<1
300–800	CS	3.4	3	<1
	CL	4.4	<1	−1

Three cloud locations, 800–900, 180–200, and 300–800 mbar, are considered using the containing small (CS) and containing large (CL) drop models from the Intercomparison of Radiation Codes in Climate Models (ICRCCM) specifications [*Fouquart et al.*, 1991]. The solar zenith angle is 53°. Also shown are the relative errors (percent) in the parameterized values due to the number of bands the spectral region is partitioned into and the method used to represent the single-scattering coalbedo in each band (see text).

correspond to these limits. Except for $0 < \nu < 2500$ cm^{-1} the error in the parameterized cloud absorption is then determined when these spectral regions are subdivided in the aforementioned manner, and the resulting flux values are summed. The degree of improvement afforded by this subdividing is analyzed and is used as a guide in determining the spectral delimiters to be used in the near-infrared. The LBL + DE cloud absorbed solar fluxes and the error in the parameterized values, for each of these four spectral regions, are presented in Tables 1a–1d.

Table 1b. Same As Table 1a Except for the Spectral Region $2500 < \nu < 4200$ cm^{-1}

Location, mbar	Type	LBL + DE, W m^{-2}	Relative Error, %: Thin: One-Band Case	Relative Error, %: Thin: Three-Band Case	Relative Error, %: Thick: One-Band Case	Relative Error, %: Thick: Three-Band Case
		$\tau_{drop} = 10$				
800–900	CS	6.6	29	22	12	12
	CL	8.3	8	9	5	8
180–200	CS	18.5	19	14	4	1
	CL	22.2	4	2	3	1
300–800	CS	17.1	12	7	4	2
	CL	19.4	4	2	2	1
		$\tau_{drop} = 1$				
800–900	CS	3.8	27	15	−6	<1
	CL	4.9	10	9	−1	3
180–200	CS	8.9	13	8	−32	−19
	CL	11.2	6	4	−11	−8
300–800	CS	15.0	7	1	2	−3
	CL	16.2	4	<1	<1	−2

For the three-band cases the partitioning is done as follows: $2500 < \nu < 2900$ cm^{-1}, $2900 < \nu < 3400$ cm^{-1}, and $3400 < \nu < 4200$ cm^{-1}.

Table 1c. Same As Table 1a Except for the Spectral Region $4200 < \nu < 8200$ cm^{-1}

Location, mbar	Type	LBL + DE, W m^{-2}	Relative Error, %: Thin: One-Band Case	Relative Error, %: Thin: Four-Band Case	Relative Error, %: Thick: One-Band Case	Relative Error, %: Thick: Four-Band Case
		$\tau_{drop} = 10$				
800–900	CS	17.2	7	<1	−5	−1
	CL	39.1	16	1	<1	<1
180–200	CS	19.7	7	<1	−10	−1
	CL	55.8	16	1	3	<1
300–800	CS	44.3	5	<1	<1	<1
	CL	70.2	10	1	1	<1
		$\tau_{drop} = 1$				
800–900	CS	9.4	−2	−1	−4	−1
	CL	13.4	1	−1	−8	−2
180–200	CS	4.0	−7	<1	−16	<1
	CL	10.5	<1	<1	−19	−2
300–800	CS	45.3	1	<1	1	<1
	CL	49.9	2	<1	−1	<1

For the four-band cases the partitioning is done as follows: $4200 < \nu < 4700$ cm^{-1}, $4700 < \nu < 5600$ cm^{-1}, $5600 < \nu < 6200$ cm^{-1}, and $6200 < \nu < 8200$ cm^{-1}.

In addition to the spectral resolution used, there are three other important factors that can affect the accuracy of the parameterized cloud absorption. The first factor is the method used to define the representative band value of the drop single-scattering albedo (thin or thick averaging) (ES96). The differences in accuracy between the two methods are investigated here by considering two drop optical depth (τ_{drop}) values, 1 and 10. The second factor is the drop model considered. The differing magnitudes of the CS and CL drop coalbedos (Figure 2b) can result in a corresponding difference in the dependence of the error on the spectral resolution. This is investigated by comparing the error in cloud absorption that results from using each drop model when the optical depth and location in the atmosphere are fixed. The third factor is the cloud location. Three cloud locations are considered: low (800–900 mbar), high (180–200 mbar), and geometrically thick (300–800 mbar) for both drop size distributions and for the two drop optical depths. These cases are chosen since they exhibit a wide range in the amount of vapor absorption both above and inside the cloud.

5.1.1. Region 0–2500 cm^{-1}. For the $0 < \nu < 2500$ cm^{-1} region, Table 1a shows the LBL + DE cloud absorbed solar flux and the error in the parameterized value, using the thin- and thick-averaging methods, for the various cases mentioned above. Considering the thin-averaging results for both drop optical depths, the error in the cloud absorbed flux is 12% or less. The CS cloud cases show a greater error; this is associated with the larger magnitude of the variation in the drop coalbedo (Figure 2b). The thick-averaging technique results in smaller errors in cloud absorption for both drop optical depths, especially for the CS cloud cases, with a maximum error of 6%. Thus the method used to derive the representative value of the

drop coalbedo becomes an important component in parameterizing the cloud absorption accurately in this region.

This degree of accuracy occurs despite the simultaneously large variations in drop and vapor absorption observed over this region (Figures 2a and 2b). There are several reasons, however, why a large drop coalbedo (>0.1 over most of this region) tends to limit the error in the parameterized cloud absorption. First, the rate of increase of drop absorptivity with coalbedo slows considerably when the coalbedo is >0.1. Thus inaccuracies arising because of spectrally averaging the drop absorptive (and reflective) properties are limited, especially for the CL cloud cases (Figure 2b). Second, the need to account for the large spectral variations in the attenuation of the solar beam by vapor above the cloud is limited. The primary concern, in this regard, is the accuracy achieved in accounting for the flux absorbed above the cloud over the entire spectral region. Third, the need to account for the large spectral variations in the absorption by vapor inside the cloud is limited. Except for the geometrically thick cloud cases this is due to the degree to which the drops dominate the total cloud absorption. Although these are all relevant factors that render further division of this region unnecessary, the most important of them all is the small value of the solar flux in this spectral interval. Thus, in spite of the strong cloud absorptivity the solar flux absorbed by the cloud is <15% of the total absorbed for the $0 < \nu < 14{,}600$ cm^{-1} region as a whole for the cases considered.

5.1.2. Region 2500–4200 cm^{-1}. For the $2500 < \nu < 4200$ cm^{-1} region, Table 1b shows the reference value and relative error in the cloud-absorbed flux for τ_{drop} of 10 and 1. Two spectral resolutions are examined: (1) the entire region is considered as a single band, and 2) the region is subdivided into three bands: $2500 < \nu < 2900$ cm^{-1}, $2900 < \nu < 3400$ cm^{-1}, and $3400 < \nu < 4200$ cm^{-1}. For the latter case the drop properties are specified and the water vapor transmission is parameterized using the ESF technique in each of these subbands. These spectral delimiters follow approximately those defined in the 24-band Slingo drop parameterization in this region and are chosen since their derivation is based on experimentation with resolving spectral variations in drop plus vapor absorption in an efficient manner [*Slingo and Schrecker*, 1982].

Considering the thin-averaging technique results for the one-band spectral resolution, the errors for the low and high CS cloud cases exceed 10% for both drop optical depths. The corresponding errors are considerably smaller for the CL cloud cases overall: 10% or less. The geometrically thick cases show the smallest errors. This is because the in-cloud vapor has the greatest fractional contribution toward the total cloud absorption, so that inaccuracies related to the specification of the representative drop coalbedo are lessened. The partitioning of the region into the three-band resolution results in smaller errors in most cases, although errors still exceed 20% for the $\tau_{\text{drop}} = 10$ low cloud case. Applying the thick-averaging technique, the one-band resolution leads to a reduction in the error compared with the one-band, thin-averaging results. This occurs for all the cloud cases, except the high $\tau_{\text{drop}} = 1$ ones. In fact, the error is also smaller than that present in the three-band, thin-averaging results for most of the cases. The three-band thick averaging results in lesser errors compared with the one-band results for most of the cases. As in the $0 < \nu < 2500$ cm^{-1} spectral region, the thick-averaging technique generally results in a better representation of cloud absorption for this spectral region, even for thin ($\tau_{\text{drop}} = 1$) clouds.

For the thin-averaging results the reduction in error between the one- and three-band resolutions can be understood by examining Figures 2a and 2b. The manner in which the spectral region is partitioned results in a separation of strong, moderate, and weakly absorbing vapor regions (Figure 2a). Although the pseudomonochromatic absorption coefficients derived from the ESF technique do not depict the spectral variation of vapor absorption in a band, they can represent the overall magnitude of the absorption strength quite well. As a result, both the spectrally dependent attenuation of the solar beam by vapor above the cloud and the spectrally dependent absorption by vapor inside the cloud are better resolved. In addition, the

Table 1d. Same As Table 1a Except for the Spectral Region $8200 < \nu < 14600$ cm^{-1}

Location, mbar	Type	LBL + DE, W m^{-2}	Relative Error, %: Thin, One-Band Case	Thin, Two-Band Case	Thick, One-Band Case	Thick, Two-Band Case
		$\tau_{drop} = 10$				
800–900	CS	14.4	<1	2	−3	<1
	CL	16.8	2	2	−9	−4
180–200	CS	1.4	−6	−8	−46	−29
	CL	4.3	5	3	−52	−30
300–800	CS	30.4	2	4	<1	3
	CL	34.5	2	3	−4	<1
		$\tau_{drop} = 1$				
800–900	CS	15.1	−1	2	−1	2
	CL	15.4	−1	2	−2	2
180–200	CS	0.5	−28	−31	−39	−37
	CL	0.8	−16	−18	−47	−36
300–800	CS	40.3	1	1	1	3
	CL	40.9	1	3	<1	3

For the two-band cases the partitioning is done as follows: $8200 < \nu < 11{,}500$ cm^{-1} and $11{,}500 < \nu < 14{,}600$ cm^{-1}.

Table 1e. Same As Table 1a Except for the Spectral Region $0 < \nu < 14{,}600$ cm^{-1}

Location, mbar	Type	LBL + DE, W m^{-2}	Relative Error, %: Thin, Low	Thin, High	Thick, Low	Thick, High
		$\tau_{drop} = 10$				
800–900	CS	41.3	8	5	<1	2
	CL	68.0	11	2	−1	<1
180–200	CS	45.1	10	6	−4	−1
	CL	89.1	11	1	−3	−1
300–800	CS	96.8	5	3	1	1
	CL	130.1	7	1	<1	<1
		$\tau_{drop} = 1$				
800–900	CS	29.6	3	4	−2	1
	CL	35.8	2	2	−4	1
180–200	CS	15.5	6	5	−24	−11
	CL	26.2	2	2	−14	−5
300–800	CS	104.0	2	2	<1	1
	CL	111.4	2	1	<1	1

"Low" refers to the lower spectral resolution partitioning in which each of the four spectral regions (Tables 1a–1d) is considered as a single band. "High" refers to the higher spectral resolution partitioning in which the last three spectral regions are further subdivided as discussed in the text.

drop properties are better represented because of the chosen spectral width of the bands (Figure 2b). Thus there results a better correlation of the spectrally varying absorption strengths of drops plus vapor. These factors are seen to contribute more notably to a reduction in the error for the CS cloud cases because of the larger variation in drop coalbedo and the greater fractional contribution by vapor toward the total cloud absorption. As in the $0 < \nu < 2500$ cm^{-1} spectral region, the strong absorptive properties of the CL drops reduce the error associated with parameterizing drop plus vapor absorption over this spectral region as well.

5.1.3. Region 4200–8200 cm^{-1}. For the $4200 < \nu < 8200$ cm^{-1} region, Table 1c shows the relative error in the cloud absorbed flux for the two drop optical depths. The two spectral resolutions examined are (1) the entire region considered as a single band and (2) the region subdivided into four bands: $4200 < \nu < 4700$ cm^{-1}, $4700 < \nu < 5600$ cm^{-1}, $5600 < \nu < 6200$ cm^{-1}, and $6200 < \nu < 8200$ cm^{-1}. The first three bands result from subdividing the $4200 < \nu < 6200$ cm^{-1} vapor absorption band, while the $6200 < \nu < 8200$ cm^{-1} region comprises yet another vapor absorbing band (Figure 2a).

Applying the thin-averaging technique, the one-band spectral resolution can yield errors of >15% for the high and low $\tau_{\text{drop}} = 10$ CL cloud cases. Contrasting with the previous spectral regions, the CL drop coalbedo is considerably smaller in this region, <0.1 (Figure 2b). There is now a greater sensitivity of the cloud absorption to inaccuracies in the spectral averaging of drop coalbedo for this drop optical depth. Further, the greater variation in the CL versus the CS coalbedo results in the generally larger errors observed. For $\tau_{\text{drop}} = 1$ the error is considerably smaller than $\tau_{\text{drop}} = 10$ for most of the cases. Because of the smaller drop coalbedo in this spectral region compared to the previous two regions, the in-cloud vapor contributes more toward the total cloud absorption for this drop optical depth. The partitioning of the region into four bands results in a significant reduction of the error, which is 1% or less for all cases. As in the previous spectral region, this manner of partitioning separates out strong, moderate, and weakly absorbing vapor regions (Figure 2a), thus improving the correlation with the corresponding variations in the drop coalbedo (Figure 2b). The smaller magnitude of the drop coalbedo makes the reductions more dramatic in this region.

For the one-band resolution the thick-averaging technique yields mostly smaller errors than the thin-averaging technique for $\tau_{\text{drop}} = 10$ but mostly larger ones for $\tau_{\text{drop}} = 1$. The error exceeds 15% for the high cloud cases. The four-band resolution yields much smaller errors, 2% or less, for both drop optical depths. There is likewise a more dramatic improvement in the parameterized cloud absorption with the increased spectral resolution in this region in comparison with the 2500–4200 cm^{-1} region, where the thick-averaging technique is applied.

5.1.4. Region 8200–14,600 cm^{-1}. Results for the $8200 < \nu < 14{,}600$ cm^{-1} spectral region are examined in Table 1d for the two drop optical depths. The two spectral resolutions examined are (1) the entire region considered as a single band and (2) the region subdivided into two bands: $8200 < \nu < 11{,}500$ cm^{-1} and $11{,}500 < \nu < 14{,}600$ cm^{-1}.

Applying the thin-averaging technique to the one-band spectral resolution yields relative errors in cloud-absorbed flux of mostly 2% or less. The high cloud cases can have considerably larger relative errors (28%), but the absolute errors are quite small. The wider spectral interval afforded in this region is due to the fact that both drops and water vapor exhibit an overall weaker absorption strength, although still manifesting substantial spectral variations (Figures 2a and 2b). Partitioning the region into two bands actually yields the same or slightly larger errors. Because of the much weaker contribution by drops toward the cloud absorption in this spectral region, the accuracy is affected more by the vapor parameterization. Except for the high cloud cases the thick-averaging technique yields nearly the same errors as the thin-averaging technique for $\tau_{\text{drop}} = 1$, with similar or slightly larger errors present for $\tau_{\text{drop}} = 10$. The high cloud cases have considerably larger errors than those derived by the thin-averaging method, >35%, but because of the small value of the reference cloud absorbed flux, the absolute differences are reduced. Overall, there does not appear to be any advantage in terms of accuracy among the differing spectral resolutions or the differing averaging techniques for this spectral region.

5.1.5. Region 0–14,600 cm^{-1}. Table 1e shows the corresponding results for the two drop optical depths for the entire $0 < \nu < 14{,}600$ cm^{-1} region. Two methods of partitioning the near-infrared spectrum are presented. "Low" refers to considering each of the four spectral regions mentioned above as a single band, and "high" refers to the subdividing done for the last three regions in the manner described above.

Applying the thin-averaging technique, the error in the cloud-absorbed flux is <12% for the low spectral resolution and <7% for the high resolution. The most significant reductions occur for the $\tau_{\text{drop}} = 10$ cases. Applying the thick-averaging technique, the error is <5%, except for the high $\tau_{\text{drop}} = 1$ cases, where they are considerably larger. Except for slight differences in the spectral band delimiters these specifications of spectral resolution and averaging technique are utilized in the ES96 multiple-band shortwave parameterization. The results here confirm the viability of their method with respect to the CS and CL drop size distributions, although more significant errors in cloud absorption can occur for high $\tau_{\text{drop}} = 1$ clouds. The higher spectral resolution reduces the error, especially for this case, but also for most of the other cases.

For the low spectral resolution, there is a clear trend toward smaller errors for the $\tau_{\text{drop}} = 1$ clouds in applying the thin-averaging technique and for the $\tau_{\text{drop}} = 10$ clouds in applying the thick-averaging technique, in accord with what is expected. Most of the contribution toward this trend comes from the $4200 < \nu < 8200$ cm^{-1} region (Table 1c). With regard to the thin-averaging technique it is of interest that the cloud absorbed flux is consistently overestimated for both spectral resolutions considered. This overestimate is also noted in the ES96 study and is attributed to the use of a linear, solar spectral-weighted mean to represent the drop single-scattering properties (particularly the single-scattering albedo) [*Ritter and Geleyn*, 1992]. Further, the partitioning done with regard to the higher spectral resolution results in a reduction of this error in accord with the results shown in ES96. From our results this is observed to occur throughout the $0 < \nu < 8200$ cm^{-1} region (Tables 1a–1c). For the $\tau_{\text{drop}} = 10$ cloud cases the thick-averaging technique does more to correct for this overestimate than does increasing the spectral resolution and applying the thin-averaging technique. This trend is also noted in ES96. For the high $\tau_{\text{drop}} = 1$ cloud cases the thick-averaging technique requires use of the higher spectral resolution to limit the error to <15%. Also, the in-cloud heating needs to be simulated as accurately as possible for high clouds in view of its effect on the temperature structure there [*Ramaswamy and*

Ramanathan, 1989]. Thus, considering both averaging techniques, high is superior to low.

5.2. Visible and Ultraviolet

In the visible and ultraviolet regions, where cloud absorption of solar radiation is considerably weaker, O_3 absorption and Rayleigh scattering become the primary quantities; the accuracy of their parameterization is affected by the choice of the spectral band delimiters. Figure 2c shows the spectral signature in the gas optical depth highlighted by the continuum nature of O_3 absorption. The spectral dependence of the clear-sky reflectivity at the TOA, displayed in Figure 2d, demonstrates the increasing importance of Rayleigh scattering in altering the tropospheric and surface absorption as wavenumber increases. The strong absorption by O_2 and O_3 in the stratosphere, for $\nu > 33{,}000$ cm^{-1}, as manifested by a significant decrease in the reflectivity, reduces the importance of Rayleigh scattering considerably. In this spectral region the relative error in the parameterized heating rate throughout the atmosphere increases monotonically with the band width. For convenience the spectral band delimiters are stipulated to be a multiple of 100 cm^{-1}, as was the case in the near-infrared. The spectral band delimiters for the new parameterization are superimposed upon these distributions in Figures 2c and 2d. Table 2 lists the numerical values of these spectral limits along with the number of pseudomonochromatic intervals within each band.

For the visible region, $14{,}600 < \nu < 24{,}600$ cm^{-1}, the resulting four band regions (11–14) are found to be sufficient for accurately parameterizing the heating rate profile as well as the reflected flux at the TOA, compared to the LBL + DA reference result. This is because the band widths are narrow enough to resolve adequately the spectral dependence of Rayleigh scattering, while the O_3 absorption is relatively weak (Figures 2c and 2d). Also, the vapor absorption in each band is weak enough so that a single pseudomonochromatic absorption coefficient is sufficient to represent it.

In the ultraviolet, for the region $24{,}600 < \nu < 43{,}300$ cm^{-1} the spectral delimiters are chosen primarily to limit the error in the parameterized stratospheric O_3 heating rate in each band. The accuracy over the region $30{,}000 < \nu < 36{,}500$ cm^{-1} is particularly affected if the spectral widths of the bands are too large because of the rapid increase in the O_3 optical depth (Figure 2c). Table 2 shows the 10 band regions (15–24) that result as a consequence. Note that there is only one pseudomonochromatic interval in each band. The resulting spectral delimiters are also adequate for accurately parameterizing the combined effects of O_3 absorption and Rayleigh scattering. Finally, for the region $43{,}300 < \nu < 57{,}600$ cm^{-1} a single band (25) is adopted, primarily for the representation of upper stratospheric heating due to the Schumann-Runge O_2 band.

Table 2. The Numerical Values of the Spectral Band Delimiters Illustrated in Figure 2 for the New Parameterization, Given in Wavenumber ν Units and in Equivalent Wavelength λ Units

Band	ν_1, cm^{-1}	ν_2, cm^{-1}	λ_1, μm	λ_2, μm	n	S_ν, W m^{-2}
1	0	2500	∞	4.00	6	12.1587
2	2,500	2,900	4.00	3.45	1	6.5070
3	2,900	3,400	3.45	2.94	5	10.7300
4	3,400	4,200	2.94	2.38	6	23.8226
5	4,200	4,700	2.38	2.13	1	19.2689
6	4,700	5,600	2.13	1.79	9	43.7116
7	5,600	6,200	1.79	1.61	5	35.7886
8	6,200	8,200	1.61	1.22	9	135.0955
9	8,200	11,500	1.22	0.870	7	239.2806
10	11,500	14,600	−0.870	0.685	8	222.9263
11	14,600	16,700	0.685	0.599	1	138.7890
12	16,700	20,000	0.599	0.500	1	182.3105
13	20,000	22,300	0.500	0.448	1	101.2186
14	22,300	24,600	0.448	0.407	1	72.2298
15	24,600	27,500	0.407	0.364	1	48.5104
16	27,500	30,000	0.364	0.333	1	28.2587
17	30,000	31,900	0.333	0.313	1	15.4827
18	31,900	33,000	0.313	0.303	1	6.0424
19	33,000	33,800	0.303	0.296	1	3.7148
20	33,800	34,500	0.296	0.290	1	3.0384
21	34,500	35,300	0.290	0.283	1	1.7734
22	35,300	36,500	0.283	0.274	1	1.9695
23	36,500	40,000	0.274	0.250	1	3.1789
24	40,000	43,300	0.250	0.231	1	1.0869
25	43,300	57,600	0.231	0.174	1	1.0672
					72	1357.96

Also shown for each band are the value of n, which is the number of pseudomonochromatic intervals needed to compute the solar absorption, and the solar flux at the top of the atmosphere (TOA).

6. Total Spectrum

Overall, the thick-averaging technique applied in conjunction with the higher spectral resolution (high) results in the least error in the parameterized cloud absorption. Thus we adopt this strategy in the multiple-band parameterization presented in this study. This results in about a 40% increase in computational expense versus the low-resolution case (low) in order to perform the shortwave calculations for the entire solar spectrum. Table 2 summarizes the spectral band delimiters used along with the number of pseudomonochromatic intervals and the solar flux at the TOA in each band. Note that the number of pseudomonochromatic intervals is >1 for bands in which the ESF technique is applied for the vapor parameterization. Twenty-five bands result of which 10 are in the near-infrared, 4 are in the visible, and 11 are in the ultraviolet region, and the number of pseudomonochromatic spectral intervals is 72. An examination of the number of pseudomonochromatic intervals for each band indicates that the majority of the computational time is taken in performing the near-infrared calculations of solar absorption. The parameterization is much less computationally intensive in the visible and ultraviolet regions of the solar spectrum.

In comparison with other formulations, there are more pseudomonochromatic intervals in our parameterization. For instance, BR92 uses 18 intervals, ES96 uses 51 intervals, and *Fu and Liou* [1992] use 54 intervals. In comparison with the ES96 study most of the additional computational expense associated with our parameterization is due to accounting for spectral variations in drop plus vapor absorption in the $4200 < \nu < 8200$ cm^{-1} region, which is treated as a single band in their formulation. Again, this is needed to assure an accurate determination of the cloud absorption in those spectral regions and hence the total solar absorption for the different drop size distributions considered here. Also, in comparison with that study, emphasis has been placed here on taking more bands in the near-infrared. This improves the representation of both gaseous and drop absorption. In that study more pseudomonochromatic intervals are used per band, which places greater emphasis on improving the representation of vapor absorption

Table 3. The Numerical Values of the Weights (a_i) and the Pseudo Absorption Coefficients (k_i) for Each ith Term Used to Compute the Transmission Due to Water Vapor in Each Absorbing Band

Band	i	a_i	k_i, cm^2 g^{-1}	P_0	m	Band	i	a_i	k_i, cm^2 g^{-1}	P_0	m
1	1	0.09312	4.00000	3	0.84	8	1	0.04476	100.00	1013	0.80
	2	0.16262	0.25461				2	0.11198	11.2462		
	3	0.14331	0.01489				3	0.11804	2.06191		
	4	0.30720	0.00052				4	0.06353	0.64058		
	5	0.27375	0.00000				5	0.08757	0.23003		
	6	0.02000	1000.00*				6	0.05028	0.08793		
2	1	1.00000	3.52400*				7	0.16530	0.01722		
3	1	0.07874	40.0000	500	0.96		8	0.34854	0.00000		
	2	0.24765	2.92354				9	0.01000	500.000*		
	3	0.37943	0.38207			9	1	0.00532	50.0000	1013	0.49
	4	0.27553	0.04629				2	0.02794	7.35556		
	5	0.01865	0.00000				3	0.04138	2.05710		
4	1	0.19212	50.0000	50	0.60		4	0.18033	0.40888		
	2	0.27513	4.75654				5	0.19552	0.06036		
	3	0.24808	0.37403				6	0.18322	0.01438		
	4	0.22628	0.02046				7	0.36629	0.00000		
	5	0.01839	0.00000			10	1	0.00361	3.00000	700	0.38
	6	0.04000	1000.00*				2	0.01292	0.70579		
5	1	1.00000	0.01443*				3	0.04997	0.15666		
6	1	0.03838	100.000	40	0.88		4	0.08942	0.03666		
	2	0.08791	6.13107				5	0.10164	0.01463		
	3	0.16378	0.83251				6	0.14075	0.00534		
	4	0.11897	0.23363				7	0.23042	0.00135		
	5	0.20201	0.05894				8	0.37127	0.00000		
	6	0.15096	0.00447			11	1	1.00000	0.00193*		
	7	0.16933	0.00036			12	1	1.00000	0.00203*		
	8	0.06466	0.00000			13	1	1.00000	0.00004*		
	9	0.00400	4000.00*			14	1	1.00000	0.00006*		
7	1	0.01606	4.00000	700	0.91						
	2	0.08166	0.28556								
	3	0.06004	0.05189								
	4	0.39433	0.00629								
	5	0.44791	0.00000								

The spectral delimiters corresponding to the band index numbers are defined in Table 2. For bands 1, 3, 4, and 6–10 these values correspond to an exponential sum fit (ESF) of the line-by-line (LBL)-derived transmission. Also shown are the reference pressure P_0 and the scaling factor m that are used to scale the water vapor amounts to determine the transmission in the inhomogeneous atmosphere for these bands.

*No scaling of the water vapor amounts is done in deriving the transmission contribution for that term.

only. Also, we have emphasized the need to represent adequately the stratospheric shortwave heating by all gases.

The set of weights and pseudomonochromatic absorption coefficients and the corresponding reference pressure P_0 and scaling factor m composing the parameterization of water vapor are shown for each band in Table 3. The value of the coefficients in the absorptivity expressions for CO_2 and O_2 in the appropriate absorbing bands are presented in Table 4. The values of the O_3 absorption coefficient and the Rayleigh scattering coefficient, along with the reference wavenumber used to compute it, are shown for each band in Table 5.

7. Accuracy of Parameterization: Clear Sky

The differences between the parameterized and reference solar absorption are now highlighted for both the new parameterization and that previously incorporated in the Geophysical Fluid Dynamics Laboratory (GFDL) SKYHI [*Hamilton et al*., 1995] general circulation model (GCM). Unless noted otherwise, an MLS atmosphere is assumed. The surface albedo is also assumed to be 0 in all the clear-sky calculations. The "older" version of the GCM uses a modified version of the Lacis-Hansen formulations for water vapor (RF92), the Lacis-Hansen prescription for O_3 and Rayleigh scattering [*Lacis and Hansen*, 1974], the *Sasamori et al*. [1972] formulation for CO_2, and a crude accounting of the Schumann-Runge O_2 heating. For the individual gases the parameterized and reference heating rate profiles are shown for a zenith angle of 53°. For the corresponding clear-sky case, involving all gases and Rayleigh scattering, the vertical profile of the relative error is displayed for three zenith angles: 0°, 53°, and 75°.

Figures 3a and 3b show the total heating rate profiles for the old and the newly developed water vapor parameterizations and the corresponding reference one, for $P > 10$ mbar, and the absolute error, respectively. Both yield somewhat comparable errors in the troposphere. In the lower stratosphere both underestimate the solar heating, but there is a further reduction of the error in the new parameterization. This is due to the additional pseudomonochromatic absorption coefficients included for that purpose. From Table 6 the maximum absolute error is 0.1 K d^{-1} for both parameterizations. However, the maximum relative error, occurring in the lower stratosphere for both parameterizations, is >60% for the old one but 30% for the new one. Thus the steps taken in developing the water vapor parameterization result in a reasonably accurate repre-

Table 4. The Numerical Values of the Coefficients Used to Determine the Transmission Due to CO_2 and O_2 in Each of the Appropriate Absorbing Bands

Band	a_x	b_x	c_x	d_x	e_x	f_x
			$x = CO_2$			
1	1.1×10^{-5}	1.0×10^{7}	4.0×10^{-1}	5.4×10^{2}	1.4×10^{3}	1.8×10^{-5}
3	1.3×10^{-3}	1.0×10^{-2}	5.0×10^{-1}	8.0×10^{-2}	1.0×10^{-3}	6.8×10^{-2}
4	4.2×10^{-3}	2.3×10^{2}	9.7×10^{-2}	1.0×10^{-1}	1.0×10^{2}	1.0×10^{-1}
6	3.2×10^{-2}	1.6×10^{0}	3.3×10^{-2}	9.1×10^{-3}	2.4×10^{0}	4.1×10^{-1}
7	6.8×10^{-1}	1.4×10^{-3}	4.9×10^{-3}	2.2×10^{-2}	1.0×10^{-4}	9.9×10^{-1}
8	7.9×10^{-4}	1.1×10^{-1}	4.6×10^{-1}	9.5×10^{-4}	1.5×10^{-1}	5.6×10^{-1}
9	7.5×10^{-2}	1.0×10^{-3}	9.4×10^{-3}	4.1×10^{0}	1.7×10^{-6}	2.8×10^{-2}
			$x = O_2$			
8	5.9×10^{-4}	1.0×10^{-4}	4.7×10^{-1}	1.0×10^{-1}	2.2×10^{-6}	8.4×10^{-2}
10	3.1×10^{-3}	6.7×10^{-3}	9.7×10^{-2}	2.1×10^{-2}	3.0×10^{-4}	2.1×10^{-1}
11	8.3×10^{-4}	1.4×10^{-5}	4.6×10^{-1}	8.8×10^{-1}	1.9×10^{-9}	7.8×10^{-1}
25	2.0×10^{-2}	8.3×10^{0}	1.5×10^{-1}			

Note that for band 25 the Schumann-Runge band, α_{2,O_2} is set to 0 (see text), and the coefficients d_{O_2}, e_{O_2}, and f_{O_2} are not defined.

sentation of the total heating rate profile in the troposphere and the lower stratosphere.

Figures 4a and 4b show the corresponding profiles for CO_2 for $P > 10^{-3}$ mbar. Note that the rapid increase of the heating rate in the upper stratosphere and the smaller tropospheric and lower stratospheric values are well accounted for in the new CO_2 parameterization. From Table 6 the maximum absolute error of 1.3 K d^{-1} occurs in the upper stratosphere. The overall maximum relative error for all three solar zenith angles is <30%; however, it is <10% for $P < 0.1$ mbar. For higher

Table 5. The Numerical Values of the O_3 Absorption Coefficient, the Reference Wavenumber (ν_{ref}) Used to Compute the Rayleigh Scattering Coefficient, and the Rayleigh Scattering Coefficient

Band	k_{O_3}, $cm^2\ g^{-1}$	ν_{ref}	$k_{Rayleigh}(P_{sfc}, T_{sfc}, \nu_{ref})$, m^{-1}
1	0	2013	1.5810×10^{-9}
2	0	2717	5.2489×10^{-9}
3	0	3173	9.7661×10^{-9}
4	0	3845	2.1070×10^{-8}
5	0	4465	3.8336×10^{-8}
6	0	5190	7.0039×10^{-8}
7	0	5914	1.1819×10^{-7}
8	0	7283	2.7239×10^{-7}
9	0	9995	9.7140×10^{-7}
10	5.0420×10^{0}	13127	2.9143×10^{-6}
11	3.7454×10^{1}	15666	5.9617×10^{-6}
12	4.0212×10^{1}	18330	1.1292×10^{-5}
13	7.0626×10^{0}	21140	2.0241×10^{-5}
14	9.6202×10^{-1}	23403	3.0771×10^{-5}
15	0	25906	4.6900×10^{-5}
16	9.7381×10^{0}	28685	7.1838×10^{-5}
17	2.3785×10^{2}	30871	9.7968×10^{-5}
18	1.5675×10^{3}	32416	1.2061×10^{-4}
19	5.3950×10^{3}	33387	1.3686×10^{-4}
20	1.2077×10^{4}	34146	1.5075×10^{-4}
21	2.7069×10^{4}	34899	1.6563×10^{-4}
22	5.2772×10^{4}	35825	1.8554×10^{-4}
23	1.1774×10^{5}	37904	2.3742×10^{-4}
24	1.0359×10^{5}	41545	3.5707×10^{-4}
25	2.4759×10^{4}	46216	5.8255×10^{-4}

The Rayleigh scattering coefficient is determined at the surface pressure P_{sfc} and temperature T_{sfc} of the midlatitude summer (MLS) profile (1013.25 mbar and 293.78 K, respectively) at the reference wavenumber for each band.

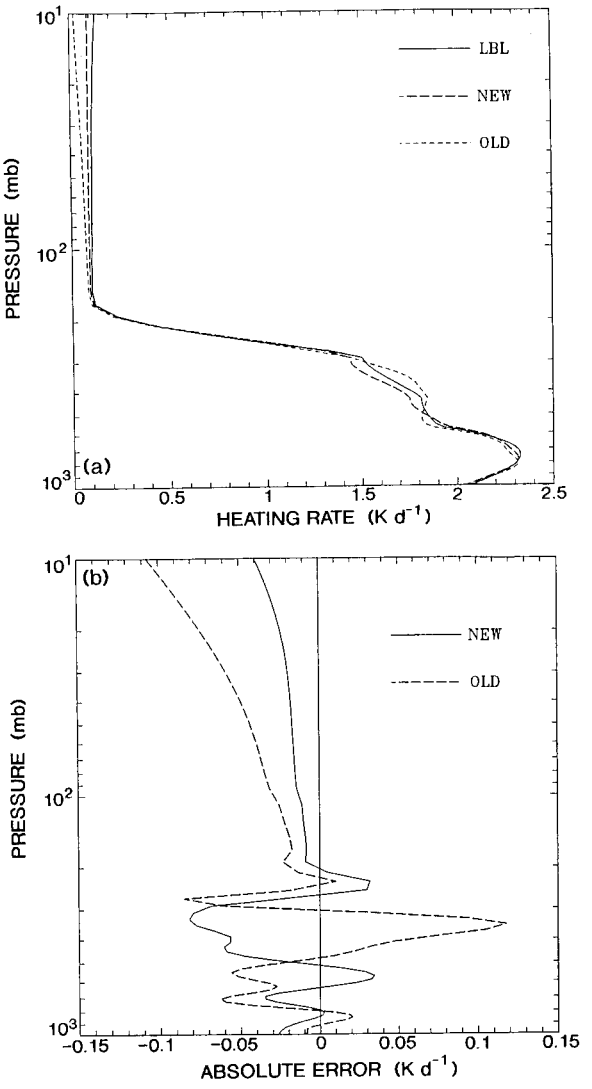

Figure 3. (a) The heating rate profiles for water vapor for the reference case and those due to the new and old (modified Lacis-Hansen [*Ramaswamy and Freidenreich*, 1992] (hereinafter referred to as RF92)) solar parameterizations and (b) the absolute error $P > 10$ mbar. A zenith angle of 53° and a midlatitude summer (MLS) atmosphere are assumed.

Table 6. The Maximum Absolute Error (AE) and the Maximum Relative Error (RE) in the Clear-Sky Heating Rate for the New and Old Individual Gas Parameterizations

	0°				53°				75°			
	New		Old		New		Old		New		Old	
Gas	AE, K d^{-1}	RE, %	AE, K d^{-1}	RE, %	AE, K d^{-1}	RE, %	AE, K d^{-1}	RE, %	AE, K d^{-1}	RE, %	AE, K d^{-1}	RE, %
H_2O	0.1	30	0.1	80	0.1	17	0.1	75	<0.1	8	<0.1	65
CO_2	1.3	29	15.0	100	1.3	29	11.0	100	1.0	29	8.0	100
O_2	0.7	20	5.8	100	0.7	18	3.8	100	0.4	17	2.3	>100
O_3	0.2	2	0.6	6	0.2	3	0.6	6	0.1	4	0.5	6

Results are shown for three solar zenith angles (Θ_0), 0°, 53°, and 75°. For water vapor the error is determined for $P > 10$ mbar only.

CO_2 amounts of 600 and 1200 ppmv a similar maximum relative error is obtained. For the old parameterization the larger stratospheric heating rates in the revised reference calculations cause a much greater underestimate than previously determined (FR93), with the absolute error being from 8 to 15 K d^{-1} in the upper stratosphere. The accurate representation of the increase in stratospheric CO_2 heating is a principal feature of the new parameterization.

The profiles for O_2 are presented in Figures 5a and 5b for $P > 10^{-3}$ mbar. The old parameterization ignores the absorption in the near-infrared and visible by O_2, resulting in a slight underestimate of the tropospheric heating. It also overestimates the heating in the upper stratosphere for $P < 0.1$ mbar, with the error increasing with height. For the new parameterization, there is a considerable reduction of this stratospheric overestimate, and the tropospheric absorption is now properly accounted. From Table 6 the new parameterization yields a maximum relative error of 20% in the heating rate for the three solar zenith angles. The maximum absolute error of 0.7 K d^{-1} is also much less than the 5.8 K d^{-1} that results in the old parameterization. The increase in the total clear-sky upper stratospheric heating due to the new CO_2 parameterization is tempered somewhat by the reduction of the large overestimate in O_2 heating present in the old one there.

Figures 6a and 6b show the corresponding results for O_3 for $P > 10^{-3}$ mbar. The old parameterization (Lacis-Hansen) agrees well with the reference results with a small underestimate in the heating. The new parameterization shows a reduction in this underestimate, yielding a closer agreement with the reference calculations. Of particular interest is the improved representation in the lower stratosphere. From Table 6 the associated maximum relative error for all three solar zenith angles is 4% for the new and 6% for the old parameterization, while the corresponding maximum absolute errors are 0.2 and 0.6 K d^{-1}, respectively.

Figure 7 displays the vertical profile of the relative error in the heating rate for the clear-sky case for the three solar zenith angles considered. For reference, note that the LBL heating rate profile for the overhead sun case is displayed in Figure 1. For all zenith angles the relative error in the new parameterization is seen to be <10%, and for most of the stratosphere it is <5%. Because of the underestimate in CO_2 heating, the old

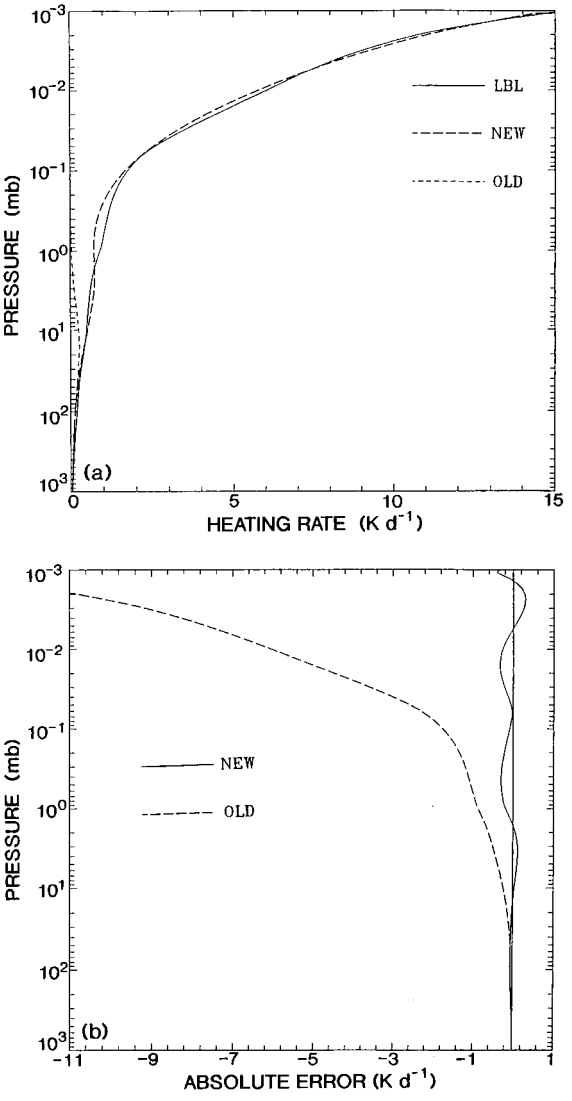

Figure 4. (a) The heating rate profiles for CO_2 for the reference case and those due to the new and old [*Sasamori et al.*, 1972] solar parameterizations and (b) the absolute error. The CO_2 amount is 346 ppmv, and a zenith angle of 53° and a MLS atmosphere are assumed.

parameterization gives >30% errors in the upper stratosphere. In the lower stratosphere, for an overhead sun both give a similar magnitude of the error, although of opposite sign, while for 53° and 75°, the new parameterization results in a much better agreement throughout the atmosphere. The improved representation of the effects due to vapor, CO_2, and O_3 contribute toward an increase in the lower stratospheric heating, which, taken together, can amount to a few tenths K d^{-1}. This would be expected to contribute nonnegligibly to an increase in the temperatures there in view of the large radiative time constant for that region. In the upper troposphere, there is a reduction of an overestimate occurring in the older parameterization. This error was a result of multiplying the individual broadband CO_2 and water vapor transmissions (FR93). The reduction of this error is due to the calculation of the transmissions over smaller spectral intervals, particularly in the neighborhood of the 2.7 μm CO_2 band (FR93). For two other McClatchey climatological profiles, tropical (TRP) and subarctic winter (SAW), the maximum relative error in the clear-sky heating rate is generally <10%; however, errors of up to 15% can occur in the upper troposphere.

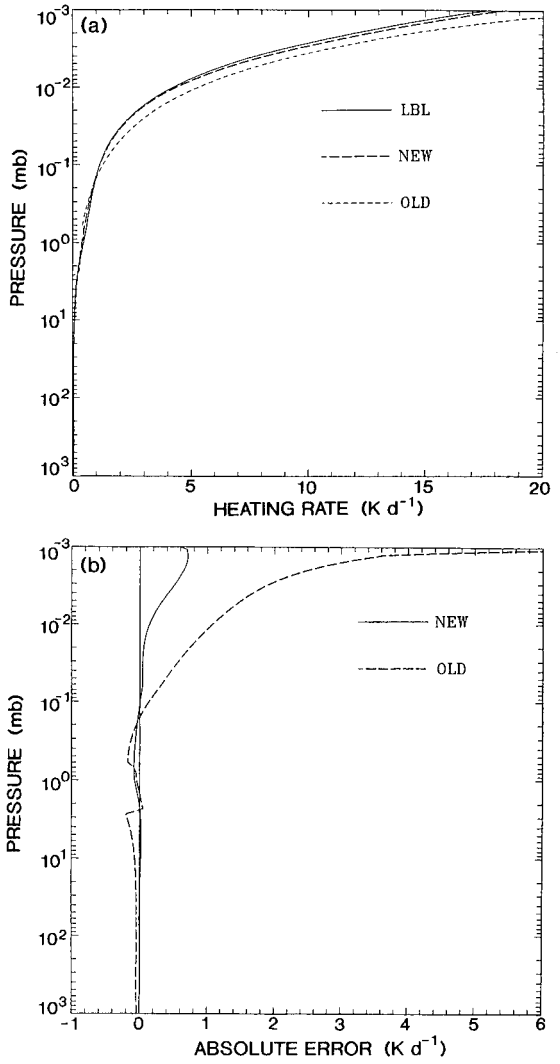

Figure 5. (a) The heating rate profiles for O_2 for the reference case and those due to the new and old solar parameterizations and (b) the absolute error. A zenith angle of 53° and a MLS atmosphere are assumed.

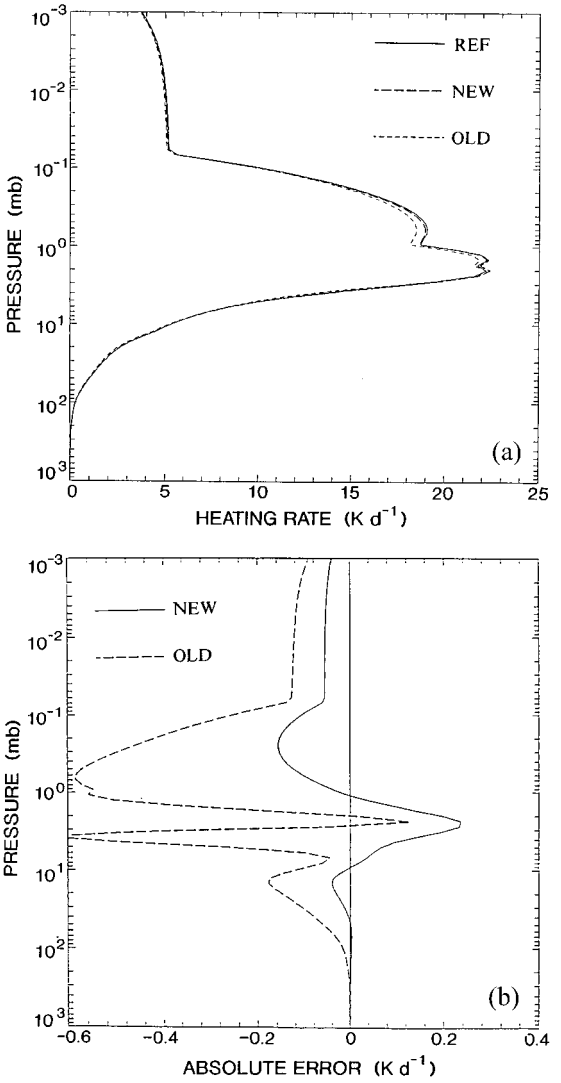

Figure 6. (a) The heating rate profiles for O_3 for the reference case and those due to the new and old [*Lacis and Hansen*, 1974] solar parameterizations and (b) the absolute error. A zenith angle of 53° and a MLS atmosphere are assumed.

To investigate further the accuracy of the new parameterization for clear skies, Table 7 presents the absorbed solar flux and the downward surface and upward TOA fluxes along with the relative error. The results are presented for the MLS, TRP, and SAW atmosphere at the three solar zenith angles. It is seen that the relative error in the clear-sky absorbed flux is generally 2%, and for the downward surface and upward TOA fluxes it is generally 1%. Thus the new parameterization meets the objective of accurately simulating the fluxes and heating rates for the clear-sky atmosphere with only a modest increase in computational expense.

8. Accuracy of Parameterization: Overcast Atmospheres

The accuracy of the new parameterization is investigated for an overcast atmosphere using the CS and CL size distributions for drops and the *Fu* [1996] formulation for ice clouds. First, a

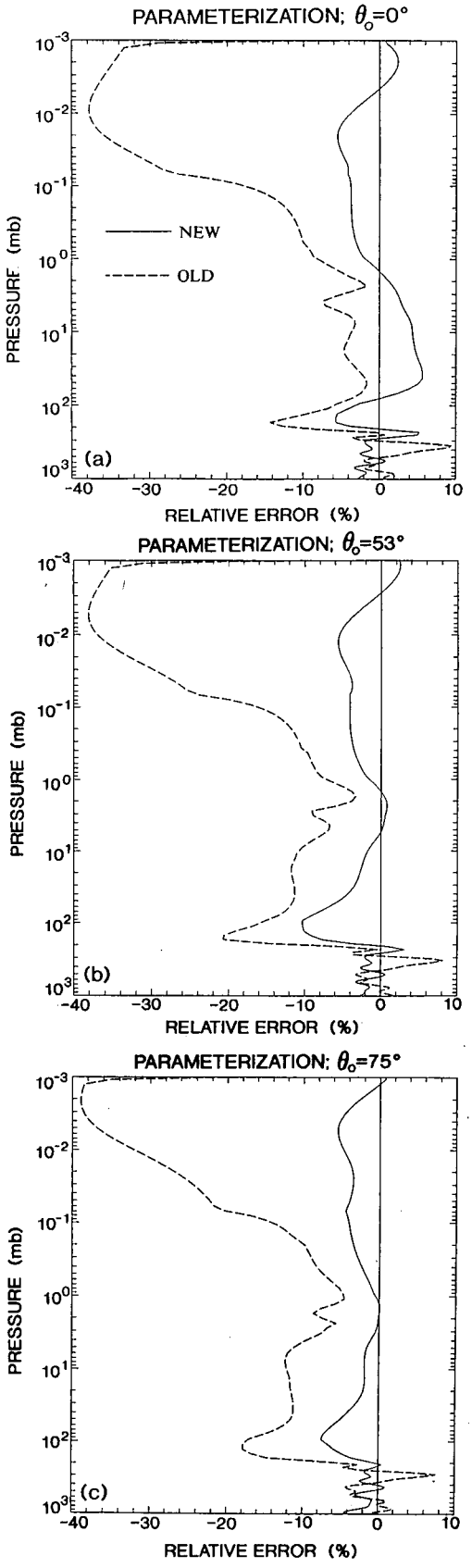

Figure 7. The relative error (percent) in the heating rate profile for the clear-sky atmosphere due to the new and old solar parameterizations for zenith angles of (a) 0°, (b) 53°, and (c) 75°. A MLS atmosphere and a CO_2 amount of 346 ppmv are assumed.

suite of cases for optical depths ranging from 1 to 100 are considered for three cloud heights, 180–200 (ice), 500–600, and 800–900 mbar (drops). The LBL + DA results are shown in terms of the percentage of the incident TOA solar irradiance in Figures 8a–8d for the absorbed flux in the cloud, the absorbed flux in the atmosphere, the downward flux at the surface, and the upward flux at the top of the atmosphere, respectively. The solar zenith angle is 51.71°, and the surface albedo is 0. The corresponding relative errors due to the new parameterization are shown in Figures 9a–9d, respectively.

The basis for the trends with increasing drop optical depth in Figure 8, and the sources of differences among the various water cloud cases for a fixed drop optical depth are described in detail by *Ramaswamy and Freidenreich* [1998]. In that study, only vapor was present along with the drops, and the spectral region considered was $0 < \nu < 18{,}000$ cm^{-1}. The results here quantify the magnitude of the fractional contribution for the entire solar spectrum and considering all gases. The patterns for the ice cloud are similar to the high water cloud case presented by *Ramaswamy and Freidenreich* [1998].

From Figures 9a and 9b the maximum relative error for the absorbed flux in the atmosphere is <5% for both the water and ice cloud cases. The maximum relative error for the absorbed flux in the cloud is <10% for the water cloud cases, but notably larger errors occur in the ice cloud cases, with values exceeding 15%. Upon further investigation it is found that most of the error occurs in the $6200 < \nu < 11{,}500$ cm^{-1} region. The larger size and coalbedo of the ice particles compared with drops in this spectral region necessitate a finer partitioning in order to improve further the approximation of the cloud absorbed flux. For the downward flux at the surface and the upward flux at the TOA, Figures 9c and 9d show a maximum error <5%, with the largest occurring for the ice cloud cases.

Geometrically thick cloud cases (i.e., containing more in-cloud vapor than those considered in Figures 8 and 9) are next investigated using the CS drop size distribution at a drop optical depth of 10; the results are listed in Table 8. The reference (LBL + DA) value for the absorbed flux in the cloud, the absorbed flux in the atmosphere, the downward flux at the surface and the upward flux at the TOA, and the relative error due to the new parameterization are presented for three cloud

Table 7. The Atmospheric Absorbed, the Downward at the Surface, and the TOA Fluxes for a Clear-Sky Atmosphere as Determined From the LBL + Doubling-Adding (DA) Calculations and the Relative Error Due to the New Parameterization

Profile	Θ_0	Absorbed, W m^{-2}	Downward, W m^{-2}	Upward, W m^{-2}
TRP	0	249.1 (−2%)	1058.8 (1%)	50.1 (<1%)
TRP	53	172.9 (−2%)	596.2 (1%)	45.7 (1%)
TRP	75	94.0 (−2%)	221.7 (1%)	35.8 (1%)
MLS	0	233.7 (−2%)	1074.8 (<1%)	49.5 (1%)
MLS	53	163.7 (−2%)	606.1 (1%)	45.1 (1%)
MLS	75	90.5 (−2%)	225.6 (1%)	35.4 (1%)
SAW	0	156.7 (−2%)	1152.8 (<1%)	48.5 (<1%)
SAW	53	114.1 (−1%)	656.6 (<1%)	44.1 (1%)
SAW	75	68.0 (−2%)	249.1 (<1%)	34.1 (2%)

Results are presented for three atmospheric profiles using *McClatchey et al.* [1972] data: TRP is the tropical, MLS is the midlatitude summer, and SAW is the subarctic winter profile, and for three solar zenith angles: 0°, 53°, and 75°. The surface albedo is 0.

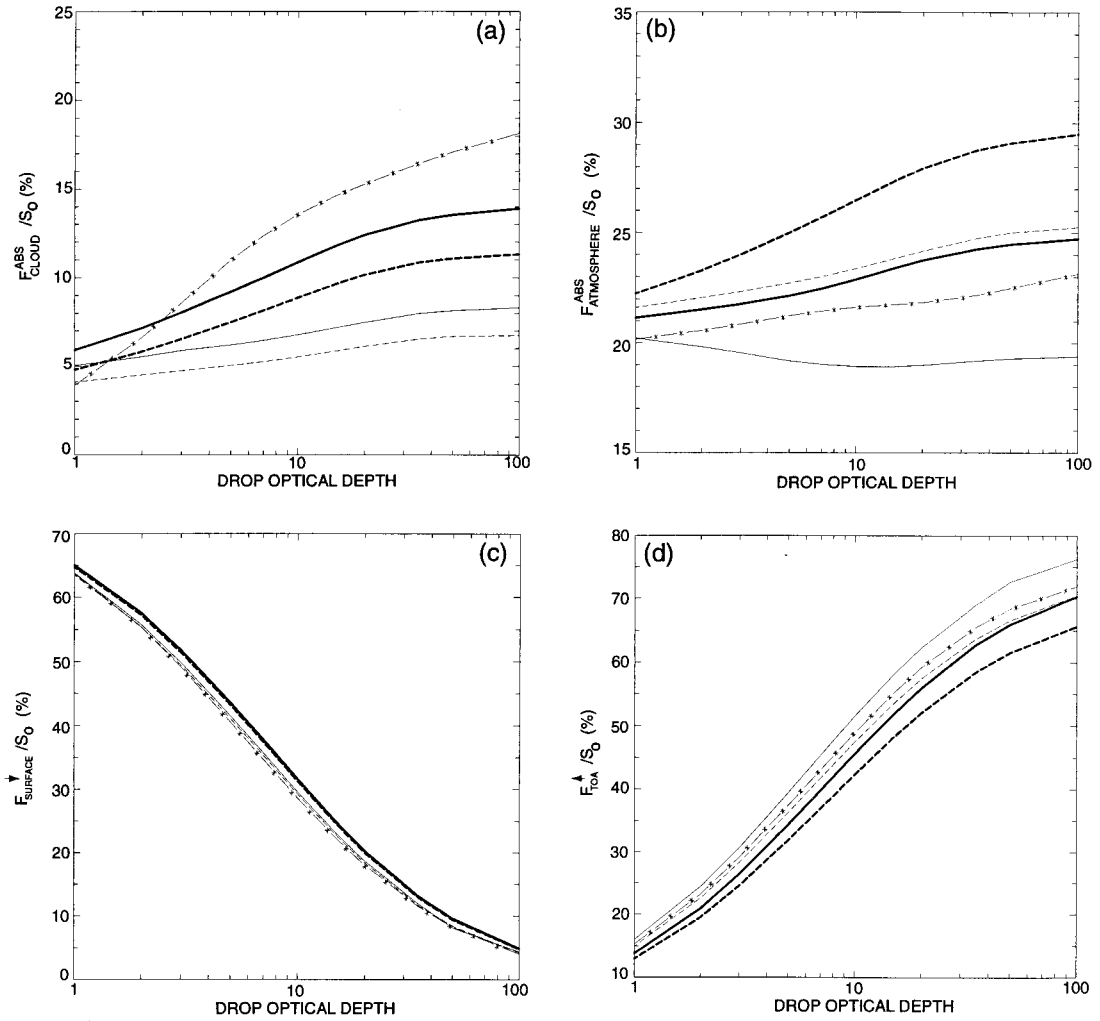

Figure 8. The reference line-by-line (LBL) and doubling-adding (DA) value for (a) the absorbed flux in the cloud, (b) the absorbed flux in the atmosphere, (c) the downward flux at the surface, and (d) the upward flux at the TOA expressed in terms of the percentage of the total solar flux at the TOA. Results are presented for Intercomparison of Radiation Codes in Climate Models (ICRCCM) [*Fouquart et al.*, 1991] drop size distributions: CS cloud at 500–600 mbar (light solid line), CS cloud at 800–900 mbar (light dashed line), CL cloud at 500–600 mbar (dark solid line), and CL cloud at 800–900 mbar (dark dashed line) for drop optical depths ranging from 1 to 100. Also shown are the results for an ice cloud using the *Fu* [1996] formulation for a generalized effective size (D_{ge}) of 100 μm at 180–200 mbar (dash-asterisks line) and for a range of optical depths from 1 to 100. A MLS atmosphere, a CO_2 amount of 346 ppmv, and a solar zenith angle of 51.71° are assumed.

locations: 180–900, 300–900, and 500–900 mbar. A solar zenith angle of 51.71° is again considered. Errors in the absorbed flux in the cloud and atmosphere are generally less than those shown in Figure 9, while those in the downward flux at the surface and the upward flux at the TOA are correspondingly greater. The errors in the individual cloudy layer heating rates (not shown) are <15%. Thus the new parameterization can represent well both the total column and individual layer absorption properties of geometrically thick clouds. Note that RF92 showed that broadband formulations can yield large variations in the error in the cloud absorbed flux with differing cloud geometrical thicknesses because of the combined effect of the errors arising in accounting for vapor absorption above and in cloudy layers. The substantial reduction of this error for geometrically thick clouds is a notable feature of the new parameterization.

For this set of cloud cases, similar maximum relative errors in the absorbed flux in the cloud and in the atmosphere are noted at other solar zenith angles, ranging from 0 to 75°. For the downward flux at the surface and the upward flux at the TOA, larger errors are found to occur than those presented in Figure 9, particularly at higher zenith angles. This is due mainly to greater inaccuracies in the DE method that can occur at these angles. Overall, the maximum errors observed are generally <10%.

To justify further the merits of the new parameterization, we select a sample of overcast sky cases that contain instances where the broadband concept can produce notably larger inaccuracies in the estimate of cloud absorption (Table 9). For the broadband parameterization we select the BR92 conceptual formulation. For this analysis we choose two cases involving a single-layer cloud and two cases involving multiple cloud

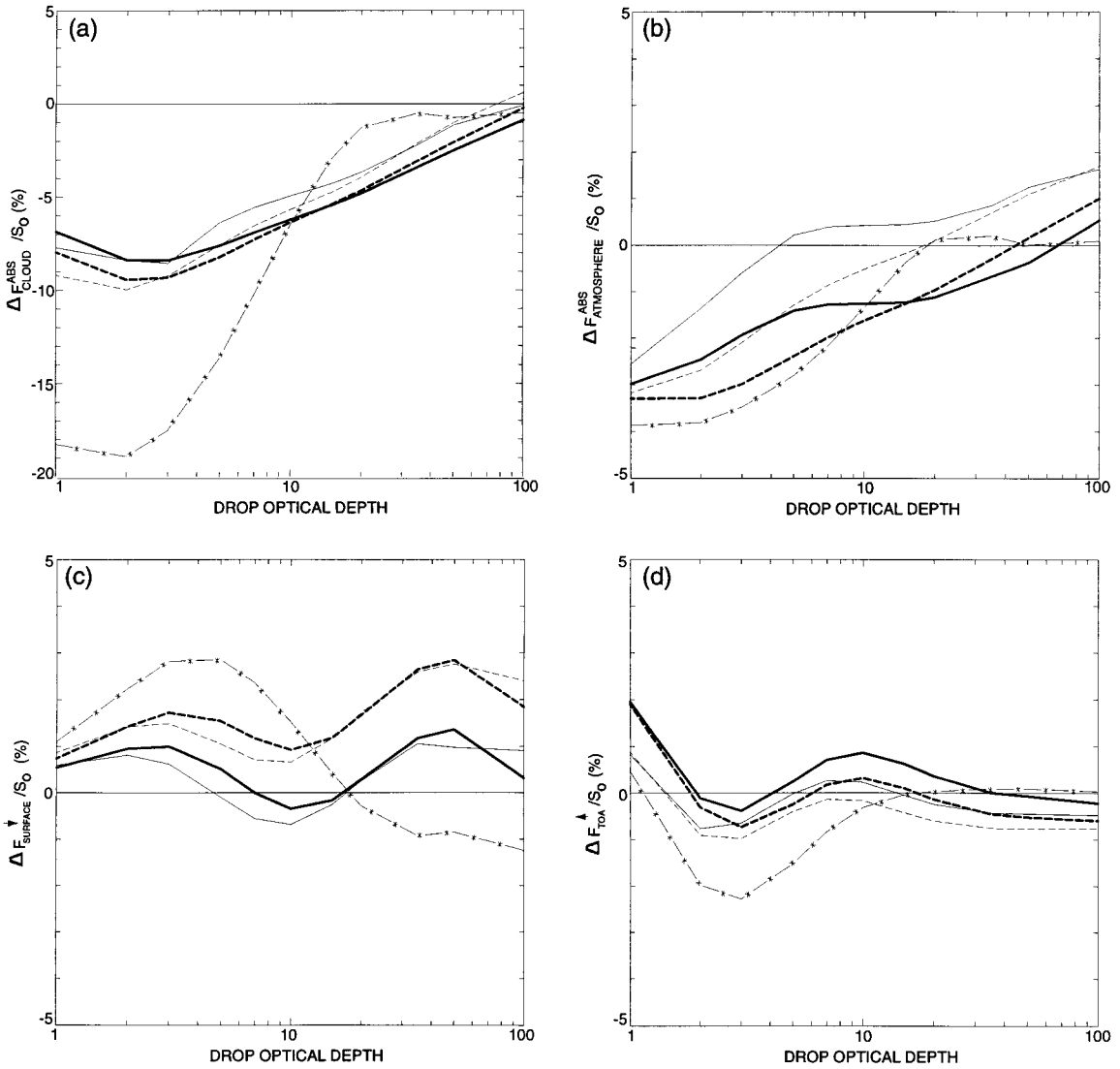

Figure 9. The relative error (percent) due to the new parameterization (i.e., with respect to reference calculations) for (a) the absorbed flux in the cloud, (b) the absorbed flux in the atmosphere, (c) the downward flux at the surface, and (d) the upward flux at the TOA for the cases presented in Figure 8.

layers. The two single-layer cases involve the same cloud properties but different surface albedos, 0 and 0.8. For the two multiple cloud layer cases one case considers the cloud layers as contiguous, and the other considers them as separated by noncloudy layers. A surface albedo of 0 is assumed in both of these cases. The *Slingo* [1989] 24-band drop single-scattering formulation is used. In Table 9 the reference (LBL + DA) result for the absorbed solar flux in the cloud(s) and in the atmosphere and the relative error due to the new parameterization (labeled PARAM) and to BR92 are presented for each of the cloud cases considered. Also shown in parentheses are the maximum relative errors in the cloudy layer heating rates for the geometrically thick cloud case in the two formulations. The corresponding LBL + DE results are included in order to make an assessment of the errors in PARAM that arise because of differences between the DE and DA scattering techniques; this is to be contrasted with that arising because of differences between the PARAM and LBL methods of treating gaseous absorption. Results are computed for two solar zenith angles, 0° and 75°.

In general, the results show minor differences in the error in the cloud absorbed flux for PARAM and LBL + DE when compared against LBL + DA. Thus the magnitude of the error in PARAM, relative to LBL + DA, is dictated mostly by the error in LBL + DE. The largest error (10%) in the cloud absorbed flux for PARAM occurs for the multiple cloud (case 4) at a zenith angle of 75° when the LBL + DE result overestimates LBL + DA and PARAM overestimates LBL + DE. A comparison of cases 1 and 2 demonstrates the accuracy of the parameterization with a large increase in the surface albedo, particularly for the overhead sun condition. The error in the individual cloud layer heating rates is $<15\%$ for the geometrically thick cloud (case 3).

For the atmospheric absorbed flux the maximum error is 6% for these cases. The corresponding differences in the downward surface and reflected TOA fluxes (not shown) between

LBL + DA and PARAM are <10% and <3%, respectively, for these cases. Here, too, the magnitude of the error in PARAM relative to LBL + DA is dictated by the error in LBL + DE; thus these errors are mostly due to the approximation of multiple scattering by the DE method.

Comparing the results using the BR92 formulation with LBL + DA, the single-layer cloud cases show a relatively good agreement with the reference results for the cloud absorption. There is a somewhat higher inaccuracy for the overhead sun condition, in contrast to PARAM. This illustrates that the increased spectral resolution associated with PARAM improves the accounting of the absorption of the diffuse beam by the cloud in instances where it accounts for a significant portion of the total cloud absorption. Overall, tests with a number of cloud cases, involving single-layer and multiple-layer (up to 5) clouds, show that the maximum error in cloud absorbed flux for the BR92 formulation are comparable with the new parameterization presented here. However, for the other cases the corresponding errors due to the BR92 formulation illustrate the greater inaccuracies that can result when applying broadband parameterizations to more complex cloud cases, with the flux differences possibly exceeding 20%. For the geometrically thick cloud (case 3) the absolute difference amounts to more than 20 W m^{-2} for the overhead Sun case. Also, for this case the maximum error in the heating rate is ~40%, and large overestimates in the heating in the topmost layers are found to contribute toward most of the overestimate in the cloud absorbed flux. Some component of these errors are likely because of the fact that the BR92 formulation uses the thin-averaging technique to represent the mean drop-scattering properties. This leads to an overestimate of cloud absorption for optically thick clouds ($\tau_{drop} = 100$) when the spectral resolution is degraded (4-band versus 24-band reference), as shown in this study and in ES96. The maximum error in the atmospheric absorbed flux (10%) occurs for the geometrically thick cloud (case 3). The results here confirm the superiority of the multiple-band technique for atmospheres containing many cloud layers that may be noncontiguous.

Overall, upon examination of several overcast sky cases (not all reported here) our new parameterization yields errors in the cloudy layer heating rates of <15%, in the cloud absorbed flux of <10%, in the atmospheric absorbed flux of <10%, in the downward surface flux of <10%, and in the reflected TOA flux of <10%. For ice clouds, larger errors in the cloud absorbed flux can occur. For the cloudy layer heating rates, this is a significant improvement from the 30% or more errors that were observed to occur using the broadband (single band in the near-infrared) parameterization in RF92, considering vapor only. The surface and TOA fluxes are likewise improved from the >10% errors that were seen to occur in RF92.

Table 8. The Reference (LBL + DA) Value for the Absorbed Flux in the Cloud, the Absorbed Flux in the Atmosphere, the Downward Flux at the Surface and the Upward Flux at the TOA, and the Relative Error Due to the New Parameterization

Location, mbar	Absorbed in Cloud, W m^{-3}	Absorbed in Atmosphere, W m^{-3}	Downward at Surface, W m^{-3}	Upward at TOA, W m^{-3}
180–900	121.1 (−2%)	161.8 (−1%)	241.5 (−9%)	438.2 (5%)
300–900	118.5 (−2%)	171.6 (−1%)	241.4 (−8%)	428.5 (5%)
500–900	99.1 (−3%)	185.5 (−1%)	241.7 (−6%)	414.3 (4%)

Results are presented for three cloud locations: 180–900, 300–900, and 500–900 mbar using the CS drop model from the ICRCCM specifications [*Fouquart et al*., 1991] at a drop optical depth of 10. A MLS atmosphere, a CO_2 amount of 346 ppmv, and a solar zenith angle of 51.71° are assumed.

Table 9. The Reference (LBL + DA) Results for the Cloud Absorbed and the Atmospheric Absorbed Solar Flux Using the *Slingo* [1989] 24-Band Drop Parameterization

Case	Cloud	LBL + DA, W m^{-2}	LBL + DE, %	PARAM, %	BR92, %
Cloud Absorbed Solar Flux: Solar Zenith Angle = 0°					
1		19.6	−2	−2	13
2		24.5	−3	−3	4
3		245.1	−5	−3 (13%)	12 (41%)
4	1	19.0	−3	−3	16
	2	86.2	−5	−4	6
	3	40.0	−3	2	14
Cloud Absorbed Solar Flux: Solar Zenith Angle = 75°					
1		10.2	−6	−7	−1
2		10.8	−6	−6	−1
3		38.7	1	3 (10%)	15 (>50%)
4	1	8.5	−5	−6	1
	2	11.0	3	5	28
	3	5.0	6	10	24
Atmospheric Absorbed Solar Flux: Solar Zenith Angle = 0°					
1		245.1	−6	−6	−4
2		299.9	<1	3	1
3		316.0	−3	1	10
4		318.4	1	5	2
Atmospheric Absorbed Solar Flux: Solar Zenith Angle = 75°					
1		64.9	4	3	1
2		72.7	5	5	2
3		70.1	−1	2	7
4		66.2	3	5	3

Also shown are the relative errors due to the LBL + DE method, the new multiple band formulation (PARAM), and a parameterization from *Briegleb* [1992] (hereinafter referred to as BR92). Results are shown for two solar zenith angles, 0° and 75°. The cloud cases are as follows: 1, 180–200 mbar, optical depth = 1, effective radius = 10 μm, and surface albedo = 0; 2, same as 1 except surface albedo = 0.8; 3, 300–800 mbar, optical depth = 100, effective radius = 15 μm, and surface albedo = 0; 4, 180–200, 480–500, and 880–900 mbar, optical depth = 1, 10, and 50, respectively, effective radius = 5, 10, and 10 μm, respectively, and surface albedo = 0. For case 4, clouds 1, 2, and 3 correspond to high, middle, and low clouds, respectively. Also shown for case 3, in parentheses, is the maximum heating rate error occuring in the model's cloudy layers.

9. Discussions

Guided by the availability of reference LBL calculations, a new multiple-band solar radiative parameterization has been developed, calibrated, and tested such that it can be considered suitable for use in atmospheric GCMs. A large and extensive number of benchmark cases are computed, analyzed, and used in developing and testing the parameterization, including different atmospheres, the effect of individual gaseous species, several different types of water and ice clouds, contiguous and noncontiguous clouds, and various solar zenith angles.

In the context of the parameterization for water vapor absorption, there are several significant aspects of this study. The availability of LBL results enables an exact determination of the functional dependence of water vapor transmission on absorber amount for a given reference pressure and tempera-

ture. Likewise, the error arising for any given ESF representation of the transmission (or absorption) in an inhomogeneous atmosphere can be assessed exactly. It is found that an accurate fitting of the functional dependence of water vapor transmission on the absorber amount does not necessarily yield an accurate parameterization of absorption in the inhomogeneous atmosphere, especially in the upper troposphere/lower stratosphere region. It is the flux convergence or heating rate, rather than transmission by itself, that constitutes the critical factor governing the accuracy of a particular ESF formulation. This is a novel aspect of the parameterization approach of this study. For each appropriate band a large catalog of ESFs are constructed in order to find a particular one that achieves a certain degree of accuracy in the heating rates with as few terms as possible. Further, the consideration of a range of reference pressures P_0 that includes stratospheric values, another unique aspect of this study, is a more rigorous test of the applicability of the scaling concept. This has been found to be necessary to reproduce accurately the reference water vapor heating rate profiles in inhomogeneous atmospheres, especially for strongly absorbing spectral bands.

With respect to the reference computation results the clear-sky heating rates are generally accurate to within 10%, and the atmospheric absorbed flux is accurate to within 2% for different atmospheric profiles and solar zenith angles. A significant improvement is made in the parameterized stratospheric heating in the new formulation compared to that previously used in the GFDL SKYHI GCM. This is owing to the greater accuracy in accounting for CO_2 and O_2 heating. Although a very high vertical resolution has been used in developing and testing the parameterization, the same accuracy in the clear-sky heating is seen to occur when applying it to much coarser resolutions typical of atmospheric GCMs (as tested in GFDL GCMs).

A major thrust of this study has been the improved representation of absorption by various types of water clouds. The factors governing the accuracy of the parameterized cloud absorption in the near-infrared have been elucidated. Foremost among these are (1) the spectral region considered, (2) the resolution adopted for representing the spectral variations in drop plus vapor absorption, and (3) the technique used to derive the representative drop properties in a band, specifically the single-scattering albedo. For both the $2500 < \nu < 4200$ cm^{-1} and $4200 < \nu < 8200$ cm^{-1} spectral regions, but especially for the latter, the error in the cloud absorbed flux is lessened significantly when each of the regions is partitioned into several bands. By carefully choosing the spectral band delimiters the large spectral variations of drops plus water vapor absorption strengths are better resolved, while the associated computational burden for the solar spectrum as a whole is increased by a modest amount. Considering the entire near-infrared spectrum and the derived representative drop coalbedos in the various bands, the thick-averaging technique yields as good as or better agreement with reference values of the cloud absorbed flux than the thin-averaging technique. The notable exception is the case of a high $\tau_{drop} = 1$ water cloud, where the thin-averaging technique is better.

For overcast atmospheres the errors have been examined for a wide range of conditions involving the ICRCCM [*Fouquart et al*., 1991] and *Slingo* [1989] drop models. Thus this formulation should be suitable for use in conjunction with many types of water drop size distributions. In this way it contrasts with the solar parameterizations presented by ES96 and BR92, where only the single-scattering parameters derived from Slingo's four-band specifications have been used for the tests. A more limited investigation of the errors has been made here for ice clouds considering the *Fu* [1996] specifications. Overall, slightly larger errors in the ice cloud absorption, versus water clouds, are possible considering the presently adopted spectral band delimiters in the near-infrared. The cloud absorbed flux is accurate to within 10%, the cloudy layer heating rates are accurate to within 15%, and the atmospheric absorbed flux is accurate to within 10%. As a consequence of a more accurate representation of the absorption, a better determination is also made of the solar flux transmitted to the surface and that reflected at the TOA. The downward surface and upward TOA fluxes are accurate to within 10%.

More complicated overcast sky cases involving multiple cloud layers illustrate not only the robustness of this parameterization but instances of how broadband parameterizations (considering the near-infrared spectral region as broad bands) can do poorly, even when they do well for simpler cases. For instance, comparisons of the multiple-band parameterization with a broadband one formulated by BR92 indicate that the cloud absorbed flux can be well represented by this broadband technique for a single cloud of limited geometrical thickness (error $<10\%$). However, for multiple and geometrically thick cloud configurations the broadband parameterization can yield a $>20\%$ error in the cloud absorbed flux and a $>40\%$ error in the cloudy layer heating rates.

In this study we have ignored the contribution of minor absorbers and their relative significance to the solar absorption. Foremost among these is NO_2. NO_2 absorption is particularly important in the presence of polluted atmospheres and convective cloud situations involving lightning. According to a recent study [*Solomon et al*., 1999], observations indicate that instantaneous enhanced absorption of at least a few W m^{-2} can occur with values up to 30 W m^{-2} possible in the presence of convective clouds, depending on the cloud properties and the vertical distribution of NO_2. Other absorbers neglected in this study are the O_2-O_2 and O_2-N_2 dimers. According to *Solomon et al*. [1998], contributions to atmospheric absorption of $\sim$2–3 W m^{-2} are estimated for a MLS atmosphere and overhead Sun. These constituents do contribute nonnegligibly to the solar absorption, and parameterizations of them will be incorporated in future versions of our shortwave GCM parameterization.

In a future study we will assess the effect of the new parameterization on the model's simulation of climate. One point in this regard may be noted: a temperature increase in the stratosphere of several degrees is expected to occur in conjunction with the increased heating due to CO_2 because of the large radiative damping times in this region. Since the old shortwave parameterization considered a broadband treatment of drop plus water vapor interactions, it is expected that significant changes in tropospheric solar absorption will also occur.

The improved accounting of solar absorption has applicability to a wide variety of problems involving radiative interactions in the troposphere and stratosphere, in accurate computations of radiative forcing in clear and overcast skies, and in climate changes due to changes in radiatively active species. The accuracy achieved for band-averaged and total solar flux transmitted to the surface and that reflected at the TOA makes the parameterization useful for comparisons with measurements of these quantities as well.

Acknowledgments. We would like to thank M. D. Schwarzkopf, C. Erlick, and two anonymous reviewers for their helpful suggestions in preparing this manuscript.

References

Briegleb, B., Delta-Eddington approximation in the NCAR Community Climate Model, *J. Geophys. Res*., *97*, 7603–7612, 1992.

Edwards, J. M., and A. Slingo, Studies with a flexible new radiation code, I, Choosing a configuration for a large-scale model, *Q. J. R. Meteorol. Soc*., *122*, 689–719, 1996.

Fouquart, Y., B. Bonnel, and V. Ramaswamy, Intercomparing shortwave radiation codes for climate studies, *J. Geophys. Res*., *96*, 8955–8968, 1991.

Freidenreich, S. M., and V. Ramaswamy, Solar absorption by CO_2, overlap with H_2O, and a parameterizations for general circulation models, *J. Geophys. Res*., *98*, 7255–7264, 1993.

Freidenreich, S. M., and V. Ramaswamy, Stratospheric temperature response to improved solar CO_2 and H_2O parameterizations, *J. Geophys. Res*., *100*, 16,721–16,725, 1995.

Fu, Q., An accurate parameterization of the solar radiative properties of cirrus clouds for climate models, *J. Clim*., *9*, 2058–2082, 1996.

Fu, Q., and K. N. Liou, On the correlated *k*-distribution method for radiative transfer in nonhomogeneous atmospheres, *J. Atmos. Sci*., *49*, 2139–2156, 1992.

Hamilton, K., R. J. Wilson, J. D. Mahlman, and L. J. Umscheid, Climatology of the SKYHI troposphere-stratosphere-mesosphere general circulation model, *J. Atmos. Sci*., *52*, 5–43, 1995.

Hunt, G. E., and I. P. Grant, Discrete space theory of radiative transfer and its application to problems in planetary atmospheres, *J. Atmos. Sci*., *26*, 963–972, 1969.

Jet Propulsion Laboratory (JPL), Chemical kinetics and photochemical data for use in stratospheric modeling: Evaluation No. 10, *JPL Publ. 92-20*, Pasadena, Calif., 1992.

Joseph, J. H., W. Wiscombe, and J. A. Weinman, The delta-Eddington approximation for radiative flux transfer, *J. Atmos. Sci*., *33*, 2452–2459, 1976.

Labs, D., and H. Neckel, Transformation of the absolute solar radiation data into the international temperature scale of 1968, *Solar Phys*., *15*, 79–87, 1970.

Lacis, A. A., and J. E. Hansen, A parameterization of the absorption of solar radiation in the Earth's atmosphere, *J. Atmos. Sci*., *31*, 118–133, 1974.

Li, J., S. M. Freidenreich, and V. Ramaswamy, Solar spectral weight at cloud tops, *J. Geophys. Res*., *102*, 11,139–11,143, 1997.

McCartney, E. J., Optics of the atmosphere: Scattering by molecules and particles, 408 pp., John Wiley, New York, 1976.

McClatchey, R. A., R. W. Fenn, J. E. A. Selby, F. E. Volz, and J. S. Garing, Optical properties of the atmosphere, *Rep. AFCRL-72-0497*, 110 pp., Hanscom Air Force Base, Bedford, Mass., 1972.

Nicolet, M., Solar spectral irradiances with their diversity between 120 and 900 nm, *Planet. Space Sci*., *37*, 1249–1289, 1989.

Ramaswamy, V., and M. M. Bowen, Effects of changes in radiatively active species upon the lower stratospheric temperatures, *J. Geophys. Res*., *99*, 18,909–18,921, 1994.

Ramaswamy, V., and S. M. Freidenreich, Solar radiative line-by-line determination of water vapor absorption and water cloud extinction in inhomogeneous atmospheres, *J. Geophys. Res*., *96*, 9133–9157, 1991.

Ramaswamy, V., and S. M. Freidenreich, A study of broadband parameterizations of the solar radiative interactions with water vapor and water drops, *J. Geophys. Res*., *97*, 11,487–11,512, 1992.

Ramaswamy, V., and S. M. Freidenreich, A high-spectral resolution study of the near-infrared solar flux disposition in clear and overcast atmospheres, *J. Geophys. Res*., *103*, 23,255–23,273, 1998.

Ramaswamy, V., and V. Ramanathan, Solar absorption by cirrus clouds and the maintenance of the tropical upper troposphere thermal structure, *J. Atmos. Sci*., *46*, 2293–2310, 1989.

Ritter, B., and J. F. Geleyn, A comprehensive radiation scheme for numerical weather prediction models with potential applications in climate simulations, *Mon. Weather Rev*., *120*, 303–325, 1992.

Rothman, L. S., et al., The HITRAN molecular database: Editions of 1991 and 1992, *J. Quant. Spectrosc. Radiat. Transfer*, *48*, 469–507, 1992.

Sasamori, T., J. London, and D. V. Hoyt, Radiation budget of the Southern Hemisphere, *Meteorol. Monogr*., *13*, 9–23, 1972.

Schwarzkopf, M. D., and S. B. Fels, The simplified exchange method revisited: An accurate, rapid method for computation of infrared cooling rates and fluxes, *J. Geophys. Res*., *96*, 9075–9096, 1991.

Slingo, A., A GCM parameterization of the shortwave radiative properties of water clouds, *J. Atmos. Sci*., *46*, 1419–1427, 1989.

Slingo, A., and H. M. Schrecker, On the shortwave radiative properties of water clouds, *Q. J. R. Meteorol. Soc*., *108*, 407–426, 1982.

Solomon, S., R. W. Portmann, R. W. Sanders, and J. S. Daniel, Absorption of solar radiation by water vapor, oxygen, and related collision pairs in the Earth's atmosphere, *J. Geophys. Res*., *103*, 3847–3858, 1998.

Solomon, S., R. W. Portmann, R. W. Sanders, J. S. Daniel, W. Madsen, B. Bartram, and E. G. Dutton, On the role of nitrogen dioxide in the absorption of solar radiation, *J. Geophys. Res*., *104*, 12,047–12,058, 1999.

Wiscombe, W. J., and J. W. Evans, Exponential-sum fitting of radiative transmission functions, *J. Comput. Phys*., *24*, 416–444, 1977.

World Meteorological Organization (WMO), Atmospheric ozone, assessment of our understanding of the processes controlling its present distribution and change, *Rep. 16*, WMO Global Ozone Res. and Monit. Proj., Washington, D. C., 1986.

S. M. Freidenreich and V. Ramaswamy, Geophysical Fluid Dynamics Laboratory, NOAA, P.O. Box 308, Princeton, NJ 08542. (smf@gfdl.gov)

(Received November 12, 1998; revised June 2, 1999;
accepted June 17, 1999.)